

Constraining Type II 2HDM in Light of LHC Higgs Searches

Baradhwaj Coleppa, Felix Kling, Shufang Su*

Department of Physics, University of Arizona, Tucson, AZ 85721, USA

Abstract

We study the implication of the LHC Higgs search results on the Type II Two Higgs-Doublet Model. In particular, we explore the scenarios in which the observed 126 GeV Higgs signal is interpreted as either the light CP-even Higgs h^0 or the heavy CP-even Higgs H^0 . Imposing both theoretical and experimental constraints, we analyze the surviving parameter regions in m_H (m_h), m_A , m_{H^\pm} , $\tan\beta$ and $\sin(\beta - \alpha)$. We further identify the regions that could accommodate a 126 GeV Higgs with cross sections consistent with the observed Higgs signal. We find that in the h^0 -126 case, we are restricted to narrow regions of $\sin(\beta - \alpha) \approx \pm 1$ with $\tan\beta$ up to 4, or an extended region with $0.55 < \sin(\beta - \alpha) < 0.9$ and $1.5 < \tan\beta < 4$. The values of m_H , m_A and m_{H^\pm} , however, are relatively unconstrained. In the H^0 -126 case, we are restricted to a narrow region of $\sin(\beta - \alpha) \sim 0$ with $\tan\beta$ up to about 8, or an extended region of $\sin(\beta - \alpha)$ between -0.8 to -0.05 , with $\tan\beta$ extended to 30 or higher. m_A and m_{H^\pm} are nearly degenerate due to $\Delta\rho$ constraints. Imposing flavor constraints shrinks the surviving parameter space significantly for the H^0 -126 case, limiting $\tan\beta \lesssim 10$, but has little effect in the h^0 -126 case. We also investigate the correlation between $\gamma\gamma$, VV and $bb/\tau\tau$ channels. $\gamma\gamma$ and VV channels are most likely to be highly correlated with $\gamma\gamma : VV \sim 1$ for the normalized cross sections.

*Electronic address: baradhwaj@email.arizona.edu, kling@email.arizona.edu, shufang@email.arizona.edu

I. INTRODUCTION

The discovery of a resonance at 126 GeV with properties consistent with the Standard Model (SM) Higgs boson in both the ATLAS [1, 2] and CMS experiments [3, 4] is undoubtedly the most significant experimental triumph of the Large Hadron Collider (LHC) to date. The nature of this particle, as regards its CP properties and couplings, are currently being established [4–6]. Though further data would undoubtedly point us in the right direction, at this point it is useful to explore the implication of the current Higgs search results on models beyond the SM. There are quite a few models that admit a scalar particle in their spectrum and many of them can have couplings and decays consistent with the SM Higgs boson. Thus it behooves us to constrain these models as much as possible with the Higgs search results at hand.

One of the simplest extensions of the SM involves enlarged Higgs sectors. This can be done by simply adding more scalar doublets, or considering Higgs sectors with more complicated representations. In the work, we will study the Two Higgs-Doublet Models (2HDM) that involve two scalar doublets both charged under the SM $SU(2)_L \times U(1)_Y$ gauge symmetries [7–10]. The neutral components of both the Higgs fields develop vacuum expectation values (vev), breaking $SU(2)_L \times U(1)_Y$ down to $U(1)_{em}$. Assuming no CP-violation in the Higgs sector, the resulting physical spectrum for the scalars is enlarged relative to the SM and includes light and heavy neutral CP-even Higgses (h^0 and H^0), charged Higgses (H^\pm), and a pseudoscalar A^0 . In addition to the masses, two additional parameters are introduced in the theory: the ratio of the vevs of the two Higgs fields ($\tan \beta$), and the mixing of the two neutral CP-even Higgses ($\sin \alpha$).

There are many types of 2HDMs, each differing in the way the two Higgs doublets couple to the fermions (for a comprehensive review, see [7]). In this work, we will be concentrating on the Type II case, in which one Higgs doublet couples to the up-type quarks, while the other Higgs doublet couples to the down-type quarks and leptons. This model is of particular interest as it shares many of the features of the Higgs sector of the Minimal Supersymmetric Standard Model (MSSM). This enables us to translate existing LHC MSSM results to this case. Before proceeding, we point out that over the last few months, there have been various studies on the 2HDM based on the recent discovery [11–24]. While most studies concentrated on finding regions of parameter space that admit $\sigma \times \text{Br}$ values reported by

the LHC experiments in various channels, some also looked at correlations between the various decay channels. The authors of Ref. [11] and Ref. [12] did the initial study of looking at the $\tan\beta - \sin\alpha$ plane where the observed Higgs signal is feasible, interpreting the discovered scalar as either the light or the heavy CP-even Higgs boson. Ref. [13–18] fit the observed Higgs signals in various 2HDM scenarios, taken into account theoretical and experimental constraints. Ref. [19] also paid careful attention to various Higgs production modes. Ref. [20] focused on the CP-violating Type II 2HDM. Ref. [21] studied the case of nearly degenerate Higgs bosons. In addition, Ref. [22, 23] investigated the possibility that the signal could correspond to the pseudoscalar A^0 - in this context, it is worth remarking that Ref. [25] considered the pseudoscalar interpretation of the observed 126 GeV resonance and found that while it is strongly disfavored, the possibility is not yet ruled out at the 5σ level.¹

In the present paper, we extended the above analyses by combining all the known experimental constraints (the LEP, Tevatron and the LHC Higgs search bounds, and precision observables) with the theoretical ones (perturbativity, unitarity, and vacuum stability), as well as flavor constraints. A unique aspect of the present work is that our analysis looks at combinations of all parameters of the theory to identify regions that survive all the theoretical and experimental constraints. We further focus on regions that could accommodate the observed Higgs signal as either the light or the heavy CP-even Higgs, and are thus interesting from a collider study perspective. This enables us to draw conclusions about correlations between different masses and mixing angles to help identify aspects of the model that warrant future study.

We start by briefly introducing the structure and parameters of the Type II 2HDM in Section II. In Sec. III, we discuss the theoretical constraints and experimental bounds, and outline our analysis methodology. In Sec. IV, we present our results for the light CP-even Higgs being the observed 126 GeV SM-like Higgs boson, looking at surviving regions in various combinations of free parameters. In Sec. V, we do the same for the heavy CP-even Higgs as the observed 126 GeV SM-like Higgs boson. In Sec. VI, we explore the implications for the Vector Boson Fusion (VBF) or VH associated production, and decays of Higgs into

¹ The latest experimental results indicate that the pseudoscalar interpretation of the 126 GeV excess is disfavored [4, 5].

$b\bar{b}$ and $\tau\tau$ channels. We conclude in Section VII.

II. TYPE II 2HDM

In this section, we briefly describe the Type II 2HDM, focusing on the particle content, Higgs couplings, and model parameters. For more details about the model, see Ref. [7] for a recent review of the theory and phenomenology of 2HDM.

A. Potential, Masses and Mixing Angles

Labeling the two $SU(2)_L$ doublet scalar fields Φ_1 and Φ_2 , the most general potential for the Higgs sector can be written down in the following form:

$$\begin{aligned} V(\Phi_1, \Phi_2) = & m_{11}^2 \Phi_1^\dagger \Phi_1 + m_{22}^2 \Phi_2^\dagger \Phi_2 - m_{12}^2 (\Phi_1^\dagger \Phi_2 + \text{h.c.}) \\ & + \frac{1}{2} \lambda_1 (\Phi_1^\dagger \Phi_1)^2 + \frac{1}{2} \lambda_2 (\Phi_2^\dagger \Phi_2)^2 + \lambda_3 (\Phi_1^\dagger \Phi_1) (\Phi_2^\dagger \Phi_2) + \lambda_4 (\Phi_1^\dagger \Phi_2) (\Phi_2^\dagger \Phi_1) \\ & + \frac{1}{2} \left\{ \lambda_5 (\Phi_1^\dagger \Phi_2)^2 + \text{h.c.} \right\} + \left\{ \left[\lambda_6 (\Phi_1^\dagger \Phi_1) + \lambda_7 (\Phi_2^\dagger \Phi_2) \right] (\Phi_1^\dagger \Phi_2) + \text{h.c.} \right\}. \end{aligned} \quad (1)$$

We impose a discrete Z_2 symmetry on the Lagrangian, the effect of which is to render $m_{12}, \lambda_6, \lambda_7 = 0^2$. Note that one consequence of requiring $m_{12} = 0$ is that there is no so called decoupling limit in which only one SM-like Higgs appears at low energy while all other Higgses are heavy and decoupled from the low energy spectrum. After electroweak symmetry breaking (EWSB): $\langle \phi_1^0 \rangle = v_1/\sqrt{2}$, $\langle \phi_2^0 \rangle = v_2/\sqrt{2}$ with $\sqrt{v_1^2 + v_2^2} = 246$ GeV, we are left with six free parameters, which can be chosen as the four Higgs masses (m_h, m_H, m_A, m_{H^\pm}), a mixing angle $\sin \alpha$ between the two CP-even Higgses, and the ratio of the two vacuum expectation values, $\tan \beta = v_2/v_1$.

Writing the two Higgs fields as:

$$\Phi_i = \begin{pmatrix} \phi_i^+ \\ (v_i + \phi_i^0 + iG_i)/\sqrt{2} \end{pmatrix}, \quad (2)$$

² Ref. [14], which also addresses similar issues as in this paper, allowed for a soft breaking of the Z_2 symmetry with $m_{12}^2 \neq 0$. In this paper, we don't consider such soft-breaking terms.

ξ_h^{VV}	$\sin(\beta - \alpha)$	ξ_H^{VV}	$\cos(\beta - \alpha)$	ξ_A^{VV}	0
ξ_h^u	$\cos \alpha / \sin \beta$	ξ_H^u	$\sin \alpha / \sin \beta$	ξ_A^u	$\cot \beta$
$\xi_h^{d,l}$	$-\sin \alpha / \cos \beta$	$\xi_H^{d,l}$	$\cos \alpha / \cos \beta$	$\xi_A^{d,l}$	$\tan \beta$

TABLE I: The multiplicative factor ξ by which the couplings of the CP-even Higgses and the CP-odd Higgs to the gauge bosons and fermions scale with respect to the SM value. The superscripts u, d, l and VV refer to the up-type quarks, down-type quarks, leptons, and WW/ZZ respectively.

the mass eigenstates of the physical scalars can be written as:

$$\begin{pmatrix} H^0 \\ h^0 \end{pmatrix} = \begin{pmatrix} \cos \alpha & \sin \alpha \\ -\sin \alpha & \cos \alpha \end{pmatrix} \begin{pmatrix} \phi_1^0 \\ \phi_2^0 \end{pmatrix}, \quad \begin{aligned} A^0 &= -G_1 \sin \beta + G_2 \cos \beta \\ H^\pm &= -\phi_1^\pm \sin \beta + \phi_2^\pm \cos \beta \end{aligned} \quad (3)$$

For our purposes, it is useful to express the quartic couplings $\lambda_{1\dots 5}$ in terms of the physical Higgs masses, $\tan \beta$ and the mixing angle α :

$$\lambda_1 = \frac{m_H^2 \cos^2 \alpha + m_h^2 \sin^2 \alpha}{v^2 \cos^2 \beta}, \quad \lambda_2 = \frac{m_H^2 \sin^2 \alpha + m_h^2 \cos^2 \alpha}{v^2 \cos^2 \beta} \quad (4)$$

$$\lambda_3 = \frac{\sin 2\alpha(m_H^2 - m_h^2) + 2 \sin 2\beta m_{H^\pm}^2}{v^2 \sin 2\beta}, \quad \lambda_4 = \frac{m_A^2 - 2m_{H^\pm}^2}{v^2}, \quad \lambda_5 = -\frac{m_A^2}{v^2}. \quad (5)$$

Imposing the perturbativity and unitarity bounds, as explained below in Sec. III A, typically leads to an upper bound on the masses of H^0 , A^0 and H^\pm . The couplings of the CP-even Higgses and CP-odd Higgs to the SM gauge bosons and fermions are scaled by a factor ξ relative to the SM value – these are presented in Table I. In order to translate the ATLAS and CMS limits, we need to pay particular attention to the couplings of the light (heavy) CP-even Higgs to the SM gauge bosons (controlling the partial decay width to WW , ZZ as well as $\gamma\gamma$ channels) and to the top quark (controlling the gluon fusion production cross section), as well as to the bottom quark (controlling the bb partial decay width, which enters the total decay width as well). From Table I, we see that the relevant couplings are proportional to $\sin(\beta - \alpha)$ ($\cos(\beta - \alpha)$), $1/\sin \beta$ and $1/\cos \beta$. Thus, even though it is customary to look at the combination of parameters $(\sin \alpha, \tan \beta)$, we present our results in Sec. IV and V using $\sin(\beta - \alpha)$ and $\tan \beta$ as the independent parameters (in addition to the masses of the physical Higgses) to manifest the effects on the Higgs couplings to gauge bosons. Using $\sin(\beta - \alpha)$ instead of $\sin \alpha$ has the additional advantage of being basis-independent, as explained in Ref. [26, 27].

III. CONSTRAINTS AND ANALYSES

A. Theoretical and Experimental Constraints

To implement the various experimental and theoretical constraints, we have employed two programs: the 2HDM Calculator (2HDMC) [28] to calculate the Higgs couplings, compute all the decay branching fractions of the Higgses, and implement all the theoretical constraints; and HiggsBounds 3.8 [29] to consistently put in all the experimental constraints on the model. Here, we briefly describe the list of theoretical and experimental bounds that are of interest.

Theoretical Constraints:

- **Vacuum Stability:** This implies that the potential should be bounded from below, which is translated to various conditions for the quartic couplings in the Higgs potential [32]: $\lambda_1 > 0$, $\lambda_2 > 0$, $\lambda_3 > -\sqrt{\lambda_1 \lambda_2}$, and $\lambda_3 + \lambda_4 - |\lambda_5| > -\sqrt{\lambda_1 \lambda_2}$. With Eqs. (4) and (5), the above requirements serve to constrain the Higgs masses and angles.
- **Perturbativity:** 2HDMC imposes constraints on the physical Higgs quartic couplings, specifically demanding that $\lambda_{h_i h_j h_k h_l} < 4\pi$ to stay inside the perturbative regime. Note that even though these are different from the λ s in the Higgs potential in Eq. (1), we can still use Eqs. (4) and (5) as rough guides to understand the perturbative bounds, as we will do in later sections to explain the features of our results. The top yukawa coupling y_t could also become nonperturbative for very small $\tan \beta$. We require the perturbativity of y_t at scales below 1 TeV, which results in $\tan \beta \gtrsim 0.35$ [33].
- **Unitarity:** It is well known that in the SM, the scattering cross section for the longitudinal W modes is unitary only if the Higgs exchange diagrams are included. Since the couplings of the Higgs are modified in the 2HDM, we need to ensure unitarity by demanding that the S matrix of *all* scattering cross sections of Higgs–Higgs and Higgs– V_L (where V_L is either W_L or Z_L) have eigenvalues bounded by 16π [34].

Experimental Constraints: The LHC experiments have searched for the SM Higgs in $\gamma\gamma$, ZZ , WW , $\tau\tau$ and $b\bar{b}$ channels. Both the ATLAS and CMS collaboration have reported the observation of a new resonance at a mass of around 126 GeV with more than 5σ significance [1–6, 35, 36]. The production cross sections and partial decay widths of the

2HDM Higgses to the various SM final states differ from that of the SM Higgs, which can be obtained using the coupling scaling factors ξ from Table I. Thus, we can identify the regions in parameter space where the signal cross sections are compatible with the Higgs signal observed at the ATLAS and CMS collaborations. We can also translate the exclusion bounds on the Higgs search to the ones in the 2HDM. We used HiggsBounds 3.8 to impose the exclusion limits from Higgs searches at the LEP and the Tevatron [37–41]. We also incorporated the latest Higgs search results at the LHC [2, 4, 35, 36, 42, 43].

Z-pole precision observables, in particular, the oblique parameters S , T (or equivalently, $\Delta\rho$, which is the deviation of $\rho \equiv \frac{m_W^2}{m_Z^2 \cos^2 \theta_W}$ from the SM value), and U [44] constrain any new physics model that couples to the W and Z . In particular, T imposes a strong constraint on the amount of custodial symmetry breaking in the new physics sector. In the case of 2HDM, the mass difference between the various Higgses are therefore highly constrained [45], which leads to interesting correlations between some of the masses, as will be demonstrated in Sec. IV and Sec. V. In our analysis, we require the contribution from extra Higgses to S and T to fall within the 90% C.L. $S - T$ contour, for a SM Higgs reference mass of 126 GeV [46]. In addition, the charged Higgs contributes to Zbb coupling [47], which has been measured precisely at the LEP via the observable $R_b = \Gamma(Z \rightarrow b\bar{b})/\Gamma(Z \rightarrow \text{hadrons})$ [48]. Imposing bounds from R_b rules out small $\tan\beta$ regions for a light charged Higgs.

We also show the effect on the available parameter spaces once bounds from flavor sector are imposed in addition to the ones described. To do this, we employed the program SuperIso 3.3 [49], which incorporates, among other things, bounds from $B \rightarrow X_s \gamma$, ΔM_{B_d} , $B^- \rightarrow \tau^- \bar{\nu}_\tau$, $D_s^\pm \rightarrow \tau^\pm (\mu^\pm) \nu$, $B \rightarrow \tau^+ \tau^-$ and $B_{d,s} \rightarrow \mu^+ \mu^-$ [50–55]. A summary of flavor bounds can be found in Ref. [56]. We have used the latest bounds either from PDG [50] or from individual experiment. To show the impact of the flavor constraints on the 2HDM parameter space, in Fig. 1, we present the regions excluded by various flavor constraints in the m_{H^\pm} versus $\tan\beta$ plane (left panel) and the m_{H^\pm} versus m_h plane (right panel). While $B \rightarrow X_s \gamma$ excludes m_{H^\pm} up to about 300 GeV for all $\tan\beta$, $B^- \rightarrow \tau^- \bar{\nu}_\tau$ and ΔM_{B_d} provide the strongest constraints at large and small $\tan\beta$, respectively. The strongest bound on the neutral Higgs mass comes from $B_s \rightarrow \mu^+ \mu^-$, which excludes m_h at about 50 GeV or lower.

In addition, we included the latest results from BaBar on $\bar{B} \rightarrow D \tau \bar{\nu}_\tau$ and $\bar{B} \rightarrow D^* \tau \bar{\nu}_\tau$ [57], which observed excesses over the SM prediction at about 2σ level. We treat the observed excesses as upper bounds and take the 95% C.L. range as $R(D) < 0.58$ and $R(D^*) < 0.39$.

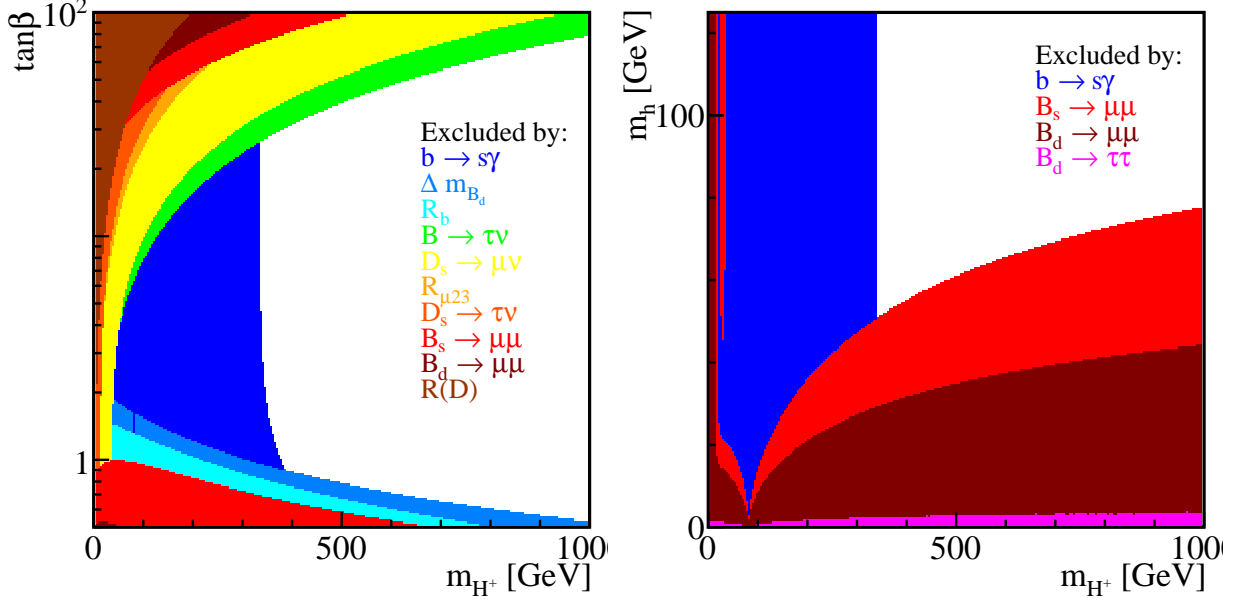


FIG. 1: Regions of parameter space excluded by various flavor constraints. The left plot shows the m_{H^\pm} versus $\tan\beta$ plane for fixed $m_h = 125$ GeV, $m_H = 400$ GeV, $m_A = 200$ GeV and $\sin(\beta - \alpha) = -0.1$. The right plot shows the m_{H^\pm} versus m_h plane for $m_A = m_{H^\pm}$, $m_H = 125$ GeV, $\tan\beta = 5$ and $\sin(\beta - \alpha) = -0.01$.

Note that as pointed out in Ref. [57], the excesses in both $R(D)$ and $R(D^*)$ can not be simultaneously explained by the Type II 2HDM [58, 59]. Other new physics contributions have to enter if the excesses in both $R(D)$ and $R(D^*)$ stay in the future. Flavor constraints on the Higgs sector are, however, typically more model-dependent. Therefore, our focus in this work is mainly on the implication of the Higgs search results on the Type II 2HDM, and we only impose the flavor bounds at the last step to indicate how the surviving regions further shrink.

B. Analysis Method

In our analysis, we considered two scenarios:

- h^0 -126 case where $m_h = 126$ GeV with $m_H > 126$ GeV,
- H^0 -126 case where $m_H = 126$ GeV with $m_h < 126$ GeV

and scanned over the entire remaining parameter space varying m_H (or m_h), m_A , m_{H^\pm} , $\tan \beta$ and $\sin(\beta - \alpha)$:

$$20 \text{ GeV} \leq m_A, m_{H^\pm} \leq 900 \text{ GeV} \quad \text{in steps of 20 GeV,} \quad (6)$$

$$-1 \leq \sin(\beta - \alpha) \leq 1 \quad \text{in steps of 0.05,} \quad (7)$$

$$\mathbf{h^0 - 126 \text{ case}} : 0.25 \leq \tan \beta \leq 5 \quad \text{in steps of 0.25,} \quad (8)$$

$$126 \text{ GeV} \leq m_H \leq 900 \text{ GeV} \quad \text{in steps of 20 GeV,} \quad (9)$$

$$\mathbf{H^0 - 126 \text{ case}} : 1 \leq \tan \beta \leq 30 \quad \text{in steps of 1,} \quad (10)$$

$$6 \text{ GeV} \leq m_h < 126 \text{ GeV} \quad \text{in steps of 5 GeV.} \quad (11)$$

In certain regions in which very few points are left after all the constraints are imposed, we generated more points with smaller steps. We used the 2HDMC 1.2beta [28] which tested if each parameter point fulfills the theoretical and experimental constraints implemented in HiggsBounds 3.8 [29]. New LHC results that are not included in HiggsBounds 3.8 were implemented in addition. In particular, the CMS results on MSSM Higgs search in $\tau\tau$ channel [43] were imposed using the cross section limits reverse-engineered from bounds in $m_A - \tan \beta$ plane for m_h^{max} scenario, as provided in HiggsBounds 4.0 [29]. We also required each parameter point to satisfy the precision constraints, in particular, S and T , as well as R_b .

We further required either h^0 or H^0 to satisfy the dominant gluon fusion cross section requirement for $\gamma\gamma$, WW and ZZ channels to accommodate the observed Higgs signal at 95% C.L. [4, 6]:

$$0.7 < \frac{\sigma(gg \rightarrow h^0/H^0 \rightarrow \gamma\gamma)}{\sigma_{\text{SM}}} < 1.5, \quad 0.6 < \frac{\sigma(gg \rightarrow h^0/H^0 \rightarrow WW/ZZ)}{\sigma_{\text{SM}}} < 1.3, \quad (12)$$

in which we have taken the tighter limits from the ATLAS and CMS results, as well as the tighter results for the WW and ZZ channel. In the last step, we imposed the flavor bounds on all points that satisfy Eq. (12) using the SuperIso 3.3 program to study the consequence of the flavor constraints.

IV. LIGHT HIGGS AT 126 GEV

A. Cross sections and Correlations

Before presenting the results of the numerical scanning of parameter regions with all the theoretical and experimental constraints imposed, let us first study the $\tan \beta$ and $\sin(\beta - \alpha)$ dependence of the cross sections for the major search channels at the LHC: $gg \rightarrow h^0 \rightarrow \gamma\gamma, WW/ZZ$. Both production cross sections and decay branching fractions are modified relative to the SM values:

$$\frac{\sigma \times \text{Br}(gg \rightarrow h^0 \rightarrow XX)}{\text{SM}} = \frac{\sigma(gg \rightarrow h^0)}{\sigma_{\text{SM}}} \times \frac{\text{Br}(h^0 \rightarrow XX)}{\text{Br}(h_{\text{SM}} \rightarrow XX)}, \quad (13)$$

for $XX = \gamma\gamma, VV$. Note that since the WW and ZZ couplings are modified the same way in the Type II 2HDM, we use VV to denote both WW and ZZ channels.

The ratio of the gluon fusion cross section normalized to the SM value can be written as:

$$\frac{\sigma(gg \rightarrow h^0)}{\sigma_{\text{SM}}} = \frac{\cos^2 \alpha}{\sin^2 \beta} + \frac{\sin^2 \alpha |A_{1/2}(\tau_b)|^2}{\cos^2 \beta |A_{1/2}(\tau_t)|^2} \quad (14)$$

$$= \left[\frac{\cos(\beta - \alpha)}{\tan \beta} + \sin(\beta - \alpha) \right]^2 + [\cos(\beta - \alpha)\tan \beta - \sin(\beta - \alpha)]^2 \frac{|A_{1/2}(\tau_b)|^2}{|A_{1/2}(\tau_t)|^2}. \quad (15)$$

The expression for the fermion loop functions $A_{1/2}(\tau_{t,b})$ can be found in Ref. [45]. The first term in Eq. (14) is the top-loop contribution, and the second term is the bottom-loop contribution. In the SM, the top-loop contributes dominantly to the gluon fusion diagram, while the bottom-loop contribution is negligibly small. The situation alters in type II 2HDM for large $\tan \beta$, when the bottom-loop contribution can be substantial due to the enhanced bottom Yukawa [11]. We also rewrite it in $\sin(\beta - \alpha)$, $\cos(\beta - \alpha)$ and $\tan \beta$ in Eq. (15) to make their dependence explicit.

In the left panel of Fig. 2, we show contours of $\sigma/\sigma_{\text{SM}}$ for the gluon fusion: $\sigma/\sigma_{\text{SM}} = 0.5$ (green), 1 (red), and 2 (blue). While contours of $\sigma/\sigma_{\text{SM}} \geq 1$ accumulate in $\sin(\beta - \alpha) \sim -1$ region, there is a wide spread of the contours for $\sin(\beta - \alpha) > 0$. For most regions of $\sin(\beta - \alpha) < 0$, $gg \rightarrow h^0$ is suppressed compared to the SM value due to cancellations between the $\cos(\beta - \alpha)$ and $\sin(\beta - \alpha)$ terms in the top Yukawa coupling, as shown in Eq. (15). Note that we have shown the plots only for $\tan \beta \leq 4$ since the model is perturbatively valid only for $\tan \beta \lesssim 4$, as will be demonstrated below in the results of the full analysis.

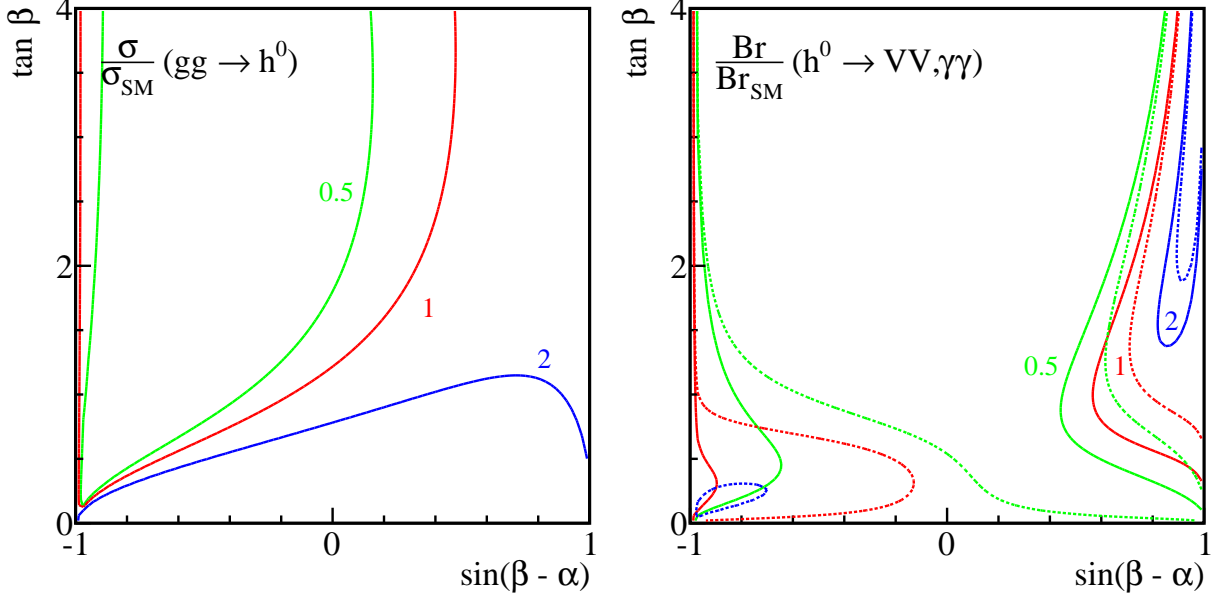


FIG. 2: The normalized $gg \rightarrow h^0$ production cross section contours (left panel) and $h^0 \rightarrow VV$ (solid lines of the right panel) and $h^0 \rightarrow \gamma\gamma$ (dashed lines of the right panel) branching fractions in the h^0 -126 case. The contour lines are $\sigma/\sigma_{\text{SM}}$, $\text{Br}/\text{Br}_{\text{SM}} = 0.5$ (green), 1 (red), and 2 (blue).

The h^0 decay branching fractions $h^0 \rightarrow VV, \gamma\gamma$ can be written approximately as

$$\frac{\text{Br}(h^0 \rightarrow XX)}{\text{Br}(h_{\text{SM}} \rightarrow XX)} = \frac{\Gamma_{XX}}{\Gamma_{\text{total}}} \times \frac{\Gamma_{\text{total}}^{\text{SM}}}{\Gamma_{XX}^{\text{SM}}} \approx \begin{cases} \frac{\sin^2(\beta-\alpha)}{\sin^2(\beta-\alpha)\text{Br}(h_{\text{SM}} \rightarrow VV) + \frac{\sin^2 \alpha}{\cos^2 \beta} \text{Br}(h_{\text{SM}} \rightarrow bb) + \dots} \\ \frac{\Gamma(h^0 \rightarrow \gamma\gamma)/\Gamma(h_{\text{SM}} \rightarrow \gamma\gamma)}{\sin^2(\beta-\alpha)\text{Br}(h_{\text{SM}} \rightarrow VV) + \frac{\sin^2 \alpha}{\cos^2 \beta} \text{Br}(h_{\text{SM}} \rightarrow bb) + \dots} \end{cases}, \quad (16)$$

where we have explicitly listed the dominant bb and WW/ZZ channels and used “+...” to indicate other sub-dominant SM Higgs decay channels.

In the right panel of Fig. 2, we show contours of $\text{Br}/\text{Br}_{\text{SM}}$ for VV (solid lines) and $\gamma\gamma$ (dashed lines) channels. Both VV and loop induced (dominantly W -loop) $\gamma\gamma$ channels exhibit similar parameter dependence on $\tan \beta$ and $\sin(\beta - \alpha)$ since both channels are dominantly controlled by the same $h^0 VV$ coupling. While contours of $\text{Br}/\text{Br}_{\text{SM}} \gtrsim 1$ appear near $\sin(\beta - \alpha) \sim \pm 1$ for unsuppressed $h^0 VV$ couplings, $h^0 \rightarrow \gamma\gamma$ shows some spread for negative $\sin(\beta - \alpha)$ and small $\tan \beta$ due to the correction to top Yukawa in the loop-induced $h^0 \gamma\gamma$ coupling.

Combining both the production and the decay branching fractions, we present the contours of $\sigma \times \text{Br}/\text{SM}$ in Fig. 3 for $\gamma\gamma$ (left panel) and VV (right panel) for $\sigma \times \text{Br}/\text{SM} = 0.5$ (green), 1 (red), and 2 (blue). Once we demand that the cross sections for these processes

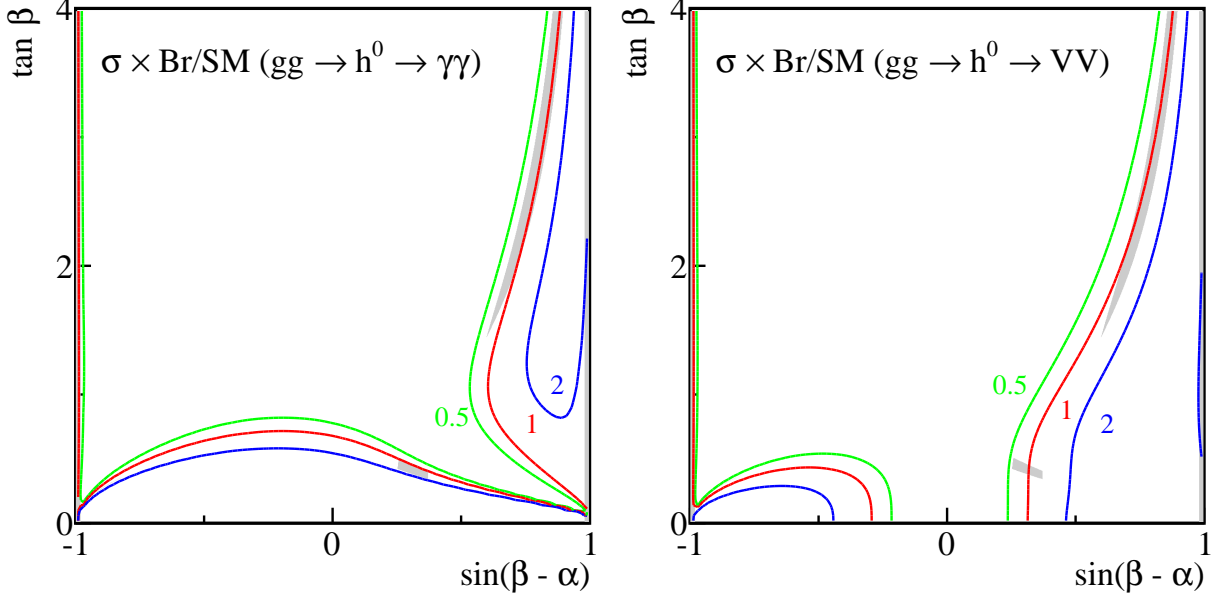


FIG. 3: $\sigma \times \text{Br}/\text{SM}$ for the processes $gg \rightarrow h^0 \rightarrow \gamma\gamma$ (left), and $gg \rightarrow h^0 \rightarrow WW/ZZ$ (right) in the h^0 -126 case. The contour lines are $\sigma \times \text{Br}/\text{SM} = 0.5$ (green), 1 (red), and 2 (blue). The shaded gray are regions where cross sections of $\gamma\gamma$ and WW/ZZ channels satisfy Eq. (12).

be consistent with the experimental observation of a 126 GeV Higgs, as given in Eq. (12), the allowed regions of parameter space split into four distinct regions, as indicated by the shaded gray areas. There are two narrow regions one each at $\sin(\beta - \alpha) = \pm 1$ (the gray regions at $\sin(\beta - \alpha) = \pm 1$ overlap with the picture frame boundary and are therefore hard to see), one extended region of $0.55 < \sin(\beta - \alpha) < 0.9$, and one low $\tan \beta$ region around $\sin(\beta - \alpha) \sim 0.3$ for $\tan \beta \sim 0.5$. Constraints from R_b disfavor this low $\tan \beta$ region and therefore we will not discuss it further. In what follows, we will display separate plots for positive and negative $\sin(\beta - \alpha)$ to show the different features that appear in these two cases.

In Fig. 4, we show the correlations for $\sigma \times \text{Br}/\text{SM}$ for the $\gamma\gamma$ channel against VV , for negative (positive) values of $\sin(\beta - \alpha)$ in the left (right) panel as a density plot. Color coding is such that the points in red are the most dense (i.e., most likely) and points in blue are the least dense (i.e., less likely). Also indicated by the small rectangular box is the normalized signal cross section range of $\gamma\gamma$ between 0.7 and 1.5, and VV channels between 0.6 and 1.3, as given in Eq. (12) [4, 6]. Note that the corresponding signal windows in $\tan \beta$ versus $\sin(\beta - \alpha)$ plane are also sketched in Fig. 3 as the shaded gray regions. For negative $\sin(\beta - \alpha)$, there are two branches: the one along the diagonal line with $\gamma\gamma : VV \sim 1$ and

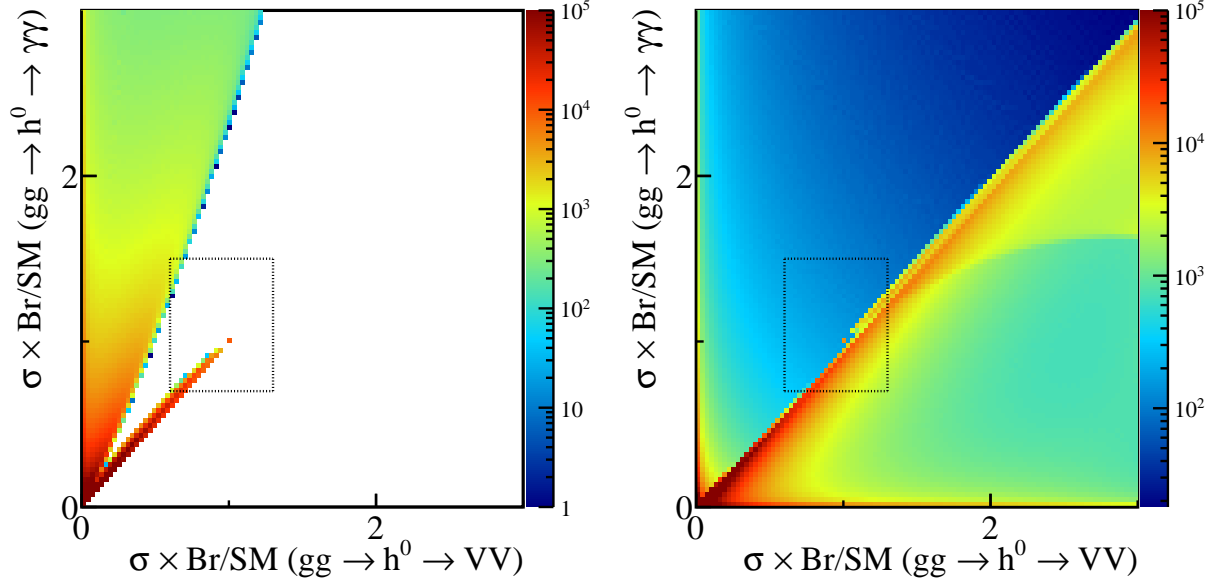


FIG. 4: $\sigma \times \text{Br}/\text{SM}$ for $gg \rightarrow h^0 \rightarrow \gamma\gamma$ versus $gg \rightarrow h^0 \rightarrow VV$ for negative $\sin(\beta - \alpha)$ (left panel), and positive $\sin(\beta - \alpha)$ (right panel) in the h^0 -126 case. Color map indicates the density of points with red being the most dense region and blue being the least dense region. Also indicated by the small rectangular box is the normalized signal cross section range of $\gamma\gamma$ between 0.7 and 1.5, and VV channels between 0.6 and 1.3 [4, 6].

$\sigma_{\gamma\gamma} \lesssim 1$, which can be mapped on to the $\sin(\beta - \alpha) = -1$ branch in Fig. 3. The other branch in the upper-half plane where $\gamma\gamma : VV \gtrsim 2$ and $\sigma_{\gamma\gamma}$ extends to 2 or larger is strongly disfavored given the current observed Higgs signal region.

For positive values of $\sin(\beta - \alpha)$, the diagonal region is the most probable, with $\gamma\gamma : VV \lesssim 1$ and $\sigma_{\gamma\gamma}$ possibly extending over a relatively large range around 1. Branches with $\sigma_{\gamma\gamma}$ or $\sigma_{VV} \sim 0$ along the axes are strongly disfavored given the current observation of the Higgs signal.

Thus we see that for all values of $\sin(\beta - \alpha)$, the VV and $\gamma\gamma$ channels are positively correlated³. Most of the points falls into $\gamma\gamma : VV \sim 1$ with the cross section of both around the SM strength. This means that an excess in the $\gamma\gamma$ channel should most likely be accompanied by an excess in the ZZ and WW channels, and this fact serves as an important piece of discrimination for this model as more data is accumulated.

³ This agrees with the results of [14].

The above analysis illustrates the cross section and decay branching fraction behavior of the light CP-even Higgs when it is interpreted as the observed 126 GeV SM-like Higgs, using the approximate formulae in Eqs. (14) - (16). Note that we have only included the usual SM Higgs decay channels in Γ_{total} in Eq. (16). While it is a valid approximation in most regions of the parameter space, it might break down when light states in the spectrum open up new decay modes or introduce large loop contributions to either $gg \rightarrow h^0$ or $h^0 \rightarrow \gamma\gamma$. In our full analysis presented below with scanning over the parameter spaces, we used the program 2HDMC, which takes into account all the decay channels of the Higgs, as well as other loop corrections to the gluon fusion production or Higgs decays to $\gamma\gamma$.

B. Parameter spaces

Fixing $m_h = 126$ GeV still leaves us with five parameters: three masses, m_H, m_A, m_{H^\pm} , and two angles $\tan\beta$ and $\sin(\beta - \alpha)$. Varying those parameters in the ranges given in Eqs. (6)-(9), we now study the remaining parameter regions satisfying all the theoretical and experimental constraints as well as regions that are consistent with the observed Higgs signal.

The left panel of Fig. 5 shows the viable regions in $\tan\beta$ versus $\sin(\beta - \alpha)$ plane when various theoretical constraints and experimental bounds are imposed sequentially. The red regions are those that satisfy all the constraints. Also shown in dark red are regions consistent with the light CP-even Higgs interpreted as the observed 126 GeV scalar particle, satisfying the cross section requirement of Eq. (12) for $gg \rightarrow h^0 \rightarrow \gamma\gamma, WW/ZZ$. The signal regions (two narrow regions at $\sin(\beta - \alpha) = \pm 1$, and one extended region with $0.55 < \sin(\beta - \alpha) < 0.9$) agree well with the shaded region in Fig. 3. The small region around $\sin(\beta - \alpha) \sim 0.3$, however, disappeared, due to the R_b constraint [47]. Regions with $\tan\beta \gtrsim 4$ are excluded by perturbative bounds since one of $\lambda_{1,2}$ becomes non-perturbative for larger value of $\tan\beta$ ($\cos\beta \rightarrow 0$), as shown in Eq. (4). Consequently, the bottom loop contribution to the gluon fusion production cross section [7] is not a major factor for the h^0 -126 case.

To further explore the flavor constraints, we show in Fig. 5 the regions enclosed by the black curves being those that survive the flavor bounds. As can clearly be seen, flavor bounds do not significantly impact the surviving signal regions.

The right panel of Fig. 5 shows the allowed region in the $\sin(\beta - \alpha) - m_H$ plane. Imposing

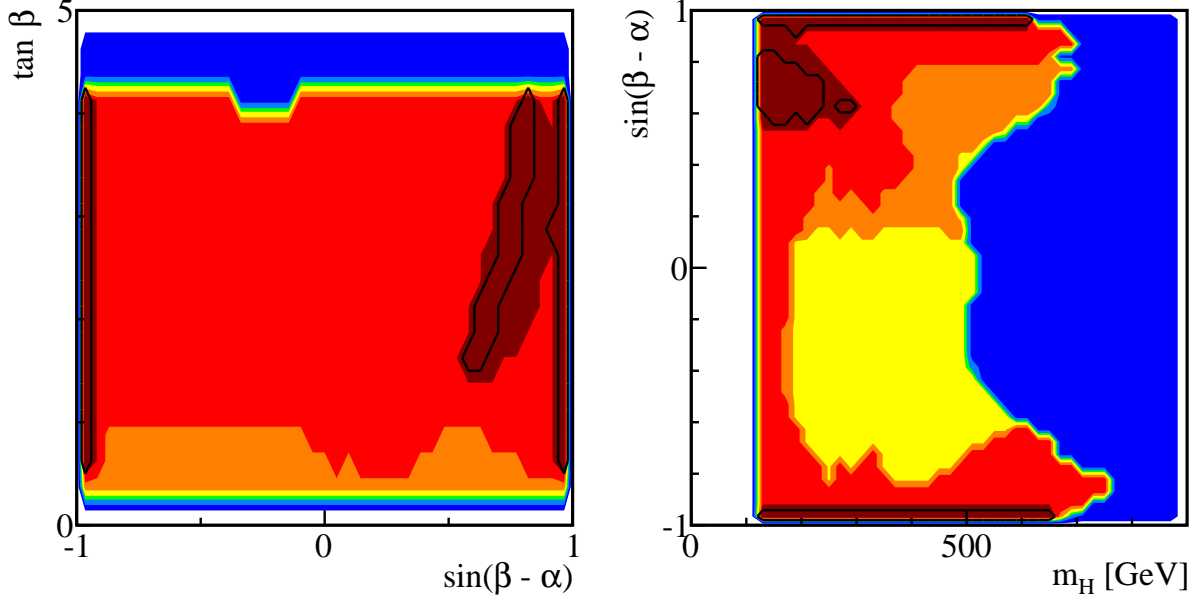


FIG. 5: Parameter regions in the h^0 -126 case for $\tan\beta$ versus $\sin(\beta - \alpha)$ (left panel) and $\sin(\beta - \alpha)$ versus m_H (right panel). We show regions excluded by stability, unitarity and perturbativity (dark blue), S and T (light blue), LEP results (green), Tevatron and LHC results (yellow), and R_b (orange). Regions that survive all the theoretical and experimental constraints are shown in red. Also shown in dark red are regions consistent with the light CP-even Higgs interpreted as the observed 126 GeV scalar resonance, satisfying the cross section requirement of Eq. (12) for $gg \rightarrow h^0 \rightarrow \gamma\gamma, WW/ZZ$. Regions enclosed by the black curves are the ones that survive the flavor constraints.

all the theoretical constraints, in particular, the perturbativity requirement, translates into an upper bound on m_H of around 750 GeV. Higgs search bounds from the LHC removes a large region in negative $\sin(\beta - \alpha)$, mostly from the stringent bounds from WW and ZZ channels for the heavy Higgs. The positive $\sin(\beta - \alpha)$ region is less constrained since $gg \rightarrow H^0 \rightarrow WW/ZZ$ are much more suppressed. R_b , in addition, excludes part of the positive $\sin(\beta - \alpha)$ region with relatively large m_H . Requiring h^0 to fit the observed Higgs signal further narrows down the favored regions, as shown in dark red. For $\sin(\beta - \alpha) = \pm 1$, m_H could be as large as 650 GeV. For $0.55 \lesssim \sin(\beta - \alpha) \lesssim 0.9$, m_H is constrained to be less than 300 GeV. The correlation between m_H and $\sin(\beta - \alpha)$ indicates that if a heavy CP-even Higgs is discovered to be between 300 and 650 GeV, $\sin(\beta - \alpha)$ is constrained to be very close to ± 1 , indicating the light Higgs has SM-like couplings to the gauge sector.

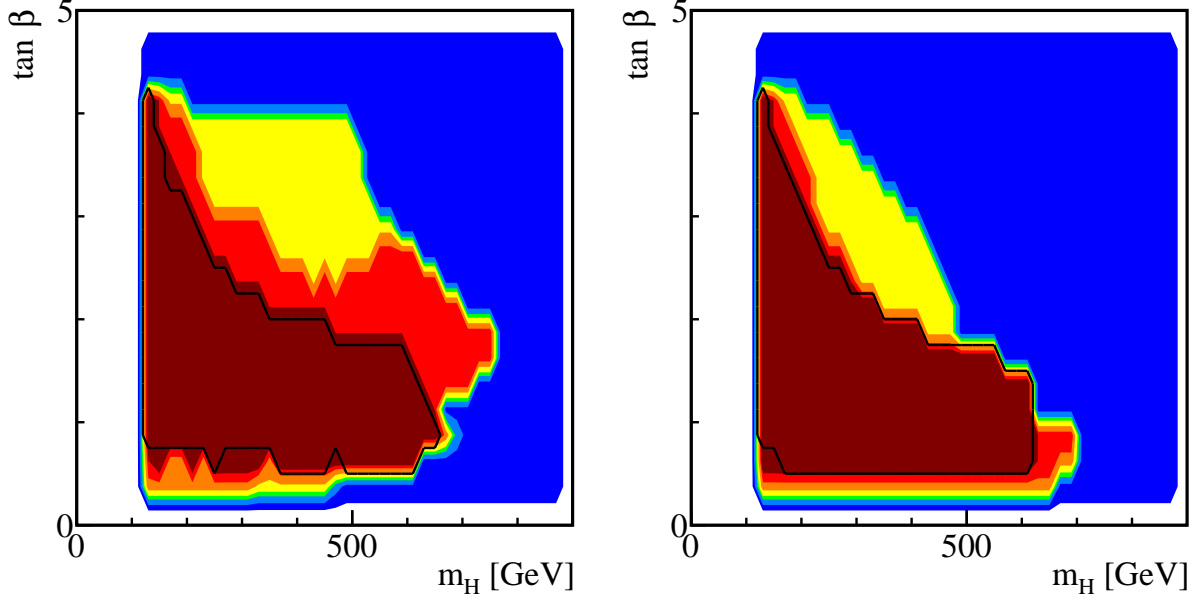


FIG. 6: Parameter regions in the h^0 -126 case for $\tan\beta$ versus m_H with $\sin(\beta - \alpha) < 0$ (left panel) and $\sin(\beta - \alpha) > 0$ (right panel). Color coding is the same as Fig. 5.

In Fig. 6, we present the parameter regions for $\tan\beta$ versus m_H with $\sin(\beta - \alpha) < 0$ (left panel) and $\sin(\beta - \alpha) > 0$ (right panel). Regions with large m_H are typically realized for small $\tan\beta$ roughly between 1 and 2. There are also noticeable difference for positive or negative $\sin(\beta - \alpha)$ for regions that survive all the experimental constraints (red regions). Negative $\sin(\beta - \alpha)$ allows larger values of $\tan\beta$ for a given mass of m_H . Small values of $\tan\beta$ is disfavored by the perturbativity of top Yukawa coupling [33], R_b [47], and the flavor constraints [56].

Fig. 7 shows the parameter regions in $\sin(\beta - \alpha)$ versus m_{H^\pm} (left panel) and m_A (right panel). For negative $\sin(\beta - \alpha)$ between -0.5 to -0.1 , only regions with $m_A < 60$ GeV survive the LHC Higgs search bounds. This is because $H^0 \rightarrow A^0 A^0$ opens up in this region, which leads to the suppression of $H^0 \rightarrow WW/ZZ$ allowing it to escape the experimental constraints. The corresponding surviving region in $120 \text{ GeV} < m_{H^\pm} < 200 \text{ GeV}$ is introduced by the correlation between m_A and m_{H^\pm} due to $\Delta\rho$ constraints. Imposing the cross section requirement for h^0 to satisfy the Higgs signal region results in three bands in both m_A and m_{H^\pm} , with masses extending all the way to about 800 GeV. Imposing the flavor constraints leaves regions with $m_{H^\pm} \gtrsim 300$ GeV viable for $\sin(\beta - \alpha) = \pm 1$ or $\sin(\beta - \alpha)$ between 0.55 and 0.9, while even smaller values for m_A remain viable at $\sin(\beta - \alpha) = \pm 1$.

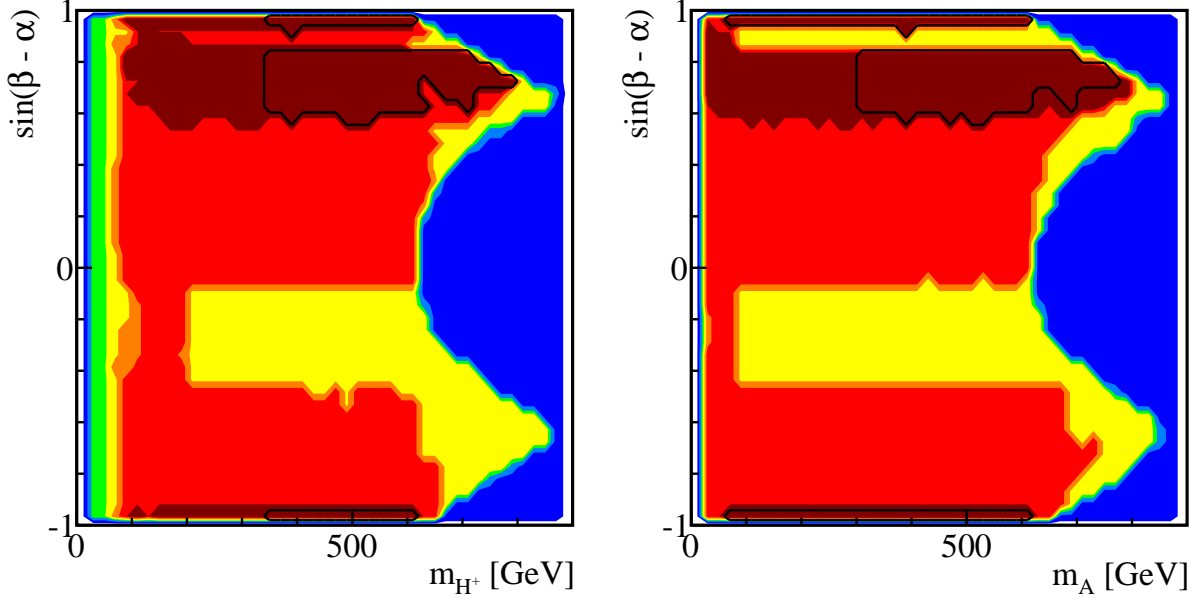


FIG. 7: Parameter regions in the h^0 -126 case for $\sin(\beta - \alpha)$ versus m_{H^\pm} (left panel) and m_A (right panel). Color coding is the same as Fig. 5.

The allowed regions in the $\tan \beta - m_{H^\pm}$ and $\tan \beta - m_A$ planes share similar features before flavor constraints are taken into account, which are shown in Fig. 8. The top two panels show the allowed regions in the $\tan \beta - m_{H^\pm}$ plane for negative and positive $\sin(\beta - \alpha)$, while the lower two panels are for $\tan \beta - m_A$. LEP places a lower bound on the charged Higgs mass around 80 GeV [39, 40]. In the signal region for $\sin(\beta - \alpha) < 0$, both m_{H^\pm} and m_A are less than about 600 GeV, while their masses could be extended to 800 GeV for $\sin(\beta - \alpha) > 0$ and $\tan \beta > 2$. The difference between the m_A range for different signs of $\sin(\beta - \alpha)$ can be explained as follows: regions with $m_A > 600$ GeV can only occur for $|\sin(\beta - \alpha)|$ between 0.4 and 0.8, as shown in the right panel of Fig. 7. The Higgs signal region of $\tan \beta$ versus $\sin(\beta - \alpha)$ (left panel of Fig. 5) shows that to simultaneously satisfy both the $\tan \beta$ range and $\sin(\beta - \alpha)$ range, only positive $\sin(\beta - \alpha)$ case survives.

Flavor bounds, as expected, have a marked effect here ruling out any value of $m_{H^\pm} \lesssim 300$ GeV for all values of $\tan \beta$, mainly due to the $b \rightarrow s\gamma$ constraint. For the CP-odd Higgs, only a corner of $\tan \beta > 2$ and $m_A < 300$ GeV is excluded, due to the combination of flavor and $\Delta\rho$ constraints. As shown in Fig. 6, only relatively light $m_H \lesssim 300$ GeV is allowed for $\tan \beta > 2$. The flavor constraints of $m_{H^\pm} \gtrsim 300$ GeV is then translated to $m_A \gtrsim 300$ GeV since the difference between m_A and m_{H^\pm} is constrained by $\Delta\rho$ considerations when both

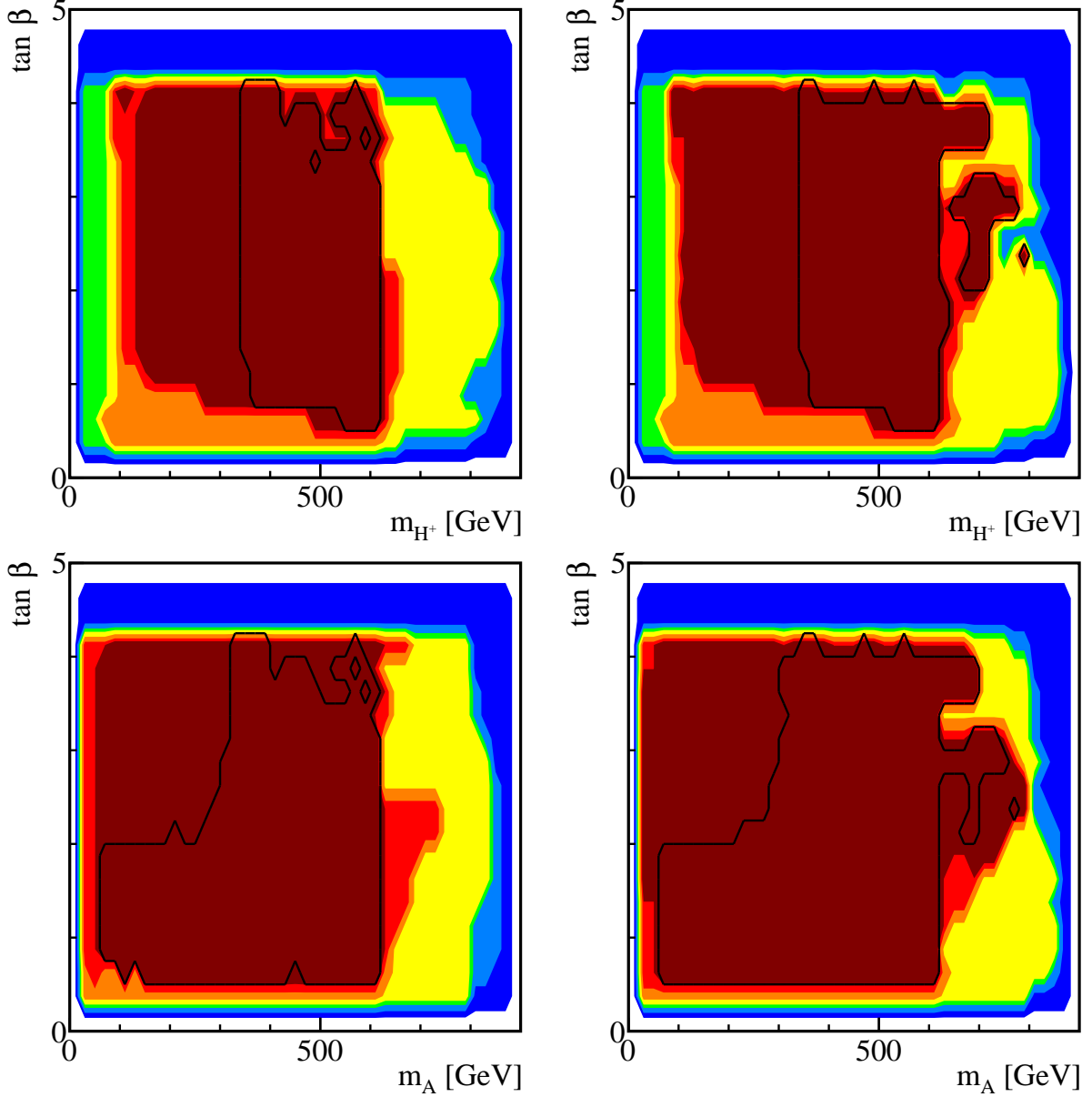


FIG. 8: Parameter regions in the h^0 -126 case for $\tan \beta$ versus m_{H^\pm} (top panels) and m_A (lower panels) with $\sin(\beta - \alpha) < 0$ (left panels) and $\sin(\beta - \alpha) > 0$ (right panels). Color coding is the same as Fig. 5.

m_h and m_H are relatively small. For $\tan \beta < 2$, m_H could be relatively high, which cancels the large contribution to $\Delta\rho$ from large m_{H^\pm} while allowing m_A to be light.

In Fig. 9, we present the parameter regions in the $m_A - m_{H^\pm}$ plane for negative and positive values of $\sin(\beta - \alpha)$. m_A and m_{H^\pm} are uncorrelated for most parts of the parameter space. For $\sin(\beta - \alpha) > 0$ when m_{A,H^\pm} could reach values larger than 600 GeV, $\tan \beta$ is at

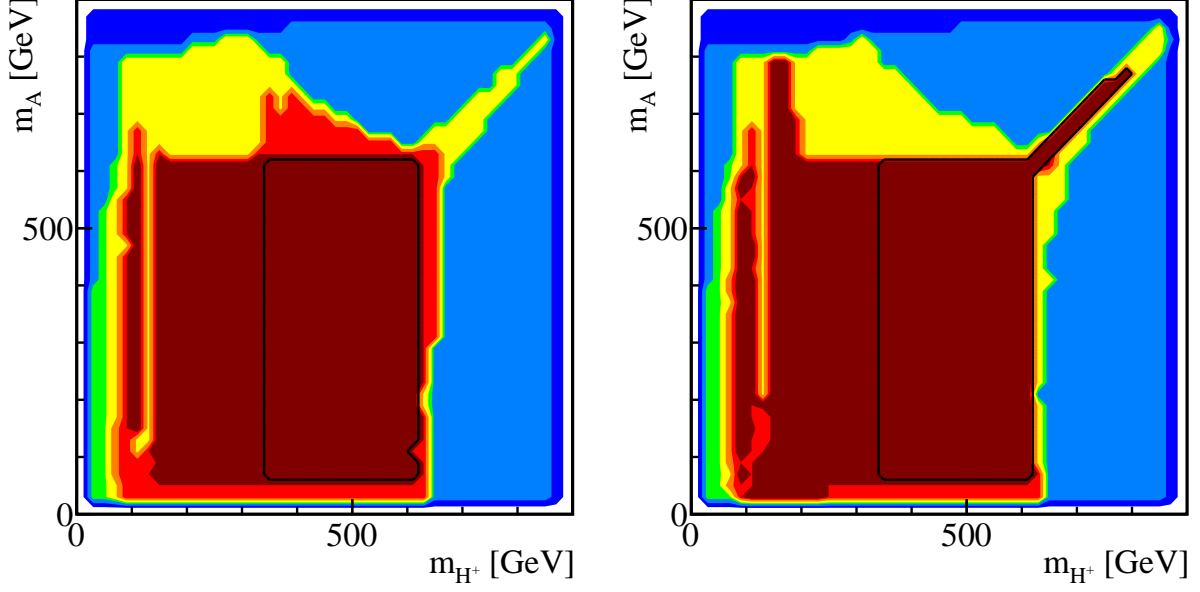


FIG. 9: Parameter regions in the h^0 -126 case for m_A versus m_{H^\pm} with $\sin(\beta - \alpha) < 0$ (left panel) and $\sin(\beta - \alpha) > 0$ (right panel). Color coding is the same as Fig. 5.

least 2 or larger (see Fig. 8). m_H is restricted to less than 300 GeV in this region, which results in a strong correlation between m_A and m_{H^\pm} due to the $\Delta\rho$ constraints.

Fig. 10 shows the parameter space in the $m_A - m_H$ plane for negative (left panel) and positive (right panel) $\sin(\beta - \alpha)$. These two masses are largely uncorrelated for either sign of $\sin(\beta - \alpha)$. Note that for $\sin(\beta - \alpha) > 0$, large m_A between 600 – 800 GeV is only possible for small values of $m_H \lesssim 250$ GeV. This is because the corresponding $\tan\beta$ is larger than 2, which bounds m_H from above. The lower-left corners excluded by flavor constraints correspond to the upper-left corners in $m_A - \tan\beta$ plots in Fig. 8, since at least one of m_A or m_H would need to be relatively heavy to cancel the contribution to $\Delta\rho$ from $m_{H^\pm} > 300$ GeV.

We conclude this section with the following comments:

- If h^0 is the 126 GeV resonance, then the $\gamma\gamma$ channel is closely correlated with WW/ZZ . Specifically, a moderate excess in $\gamma\gamma$ should be accompanied by a corresponding excess in WW/ZZ .
- The combination of all theoretical constraints requires $\tan\beta \lesssim 4$. Therefore, the bottom-loop enhancement to the gluon fusion [7] is never a major factor. Regions of $\sin(\beta - \alpha)$ and $\tan\beta$ are highly restricted once we require the light CP-even Higgs to

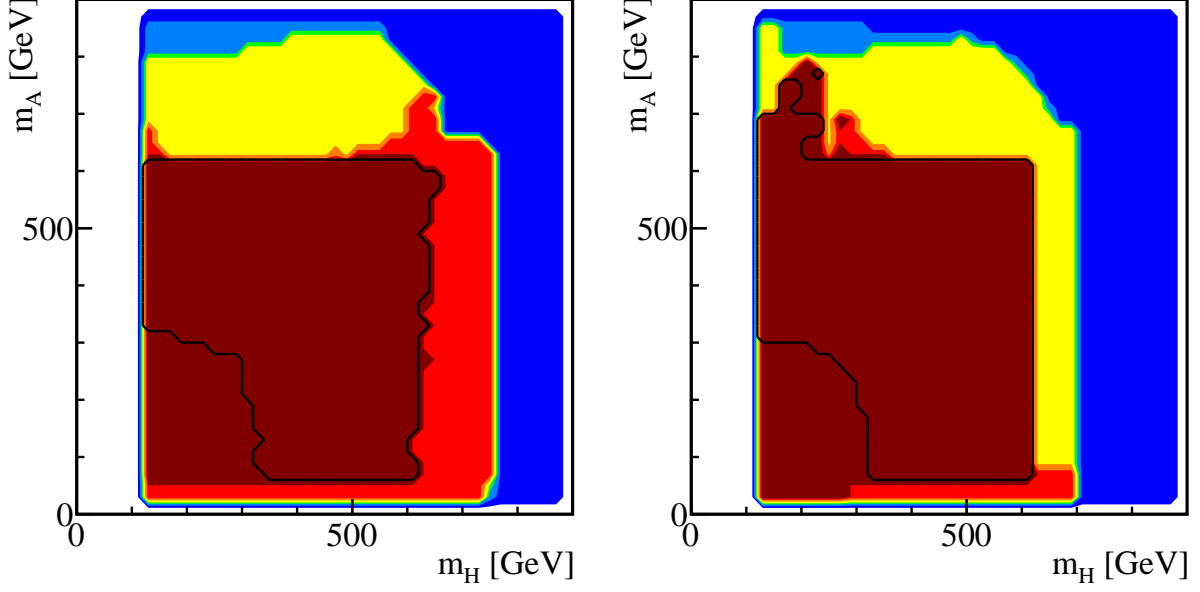


FIG. 10: Parameter regions in the h^0 -126 case for m_A versus m_H with $\sin(\beta - \alpha) < 0$ (left panel) and $\sin(\beta - \alpha) > 0$ (right panel). Color coding is the same as Fig. 5.

be the observed 126 GeV scalar particle: $\tan \beta$ between 0.5 to 4 for $\sin(\beta - \alpha) = \pm 1$, $\tan \beta$ between 1.5 to 4 for $0.55 < \sin(\beta - \alpha) < 0.9$. The masses of the other Higgses, m_H , m_A , and m_{H^\pm} , however, are largely unrestricted and uncorrelated, except for the region where $\sin(\beta - \alpha) > 0$ and $m_{A,H^\pm} \gtrsim 600$ GeV, which exhibits a strong correlation between these two masses.

- The discovery of any one of the extra scalars can largely narrow down the parameter space, in particular, if the masses of those particles are relatively high.
- Flavor bounds do not change the allowed parameter space much except for the charged Higgs mass, which is constrained to lie above 300 GeV.

V. HEAVY HIGGS AT 126 GEV

A. Cross sections and Correlations

It is possible that the 126 GeV resonance discovered at the LHC corresponds to the heavier of the two CP-even Higgses, H^0 . There are a few noticeable changes for the heavy H^0 being the SM-like Higgs boson. First of all, since the coupling of the heavy Higgs to a

gauge boson pair is scaled by a factor of $\cos(\beta - \alpha)$ as opposed to $\sin(\beta - \alpha)$, demanding SM-like cross sections for H^0 forces us to consider $\sin(\beta - \alpha) \sim 0$, as opposed to $\sin(\beta - \alpha) \sim \pm 1$ in the h^0 -126 case. Secondly, as will be demonstrated below, the bottom contribution to the gluon fusion production could be significantly enhanced since the range of $\tan \beta$ could be much larger compared to the h^0 -126 case.

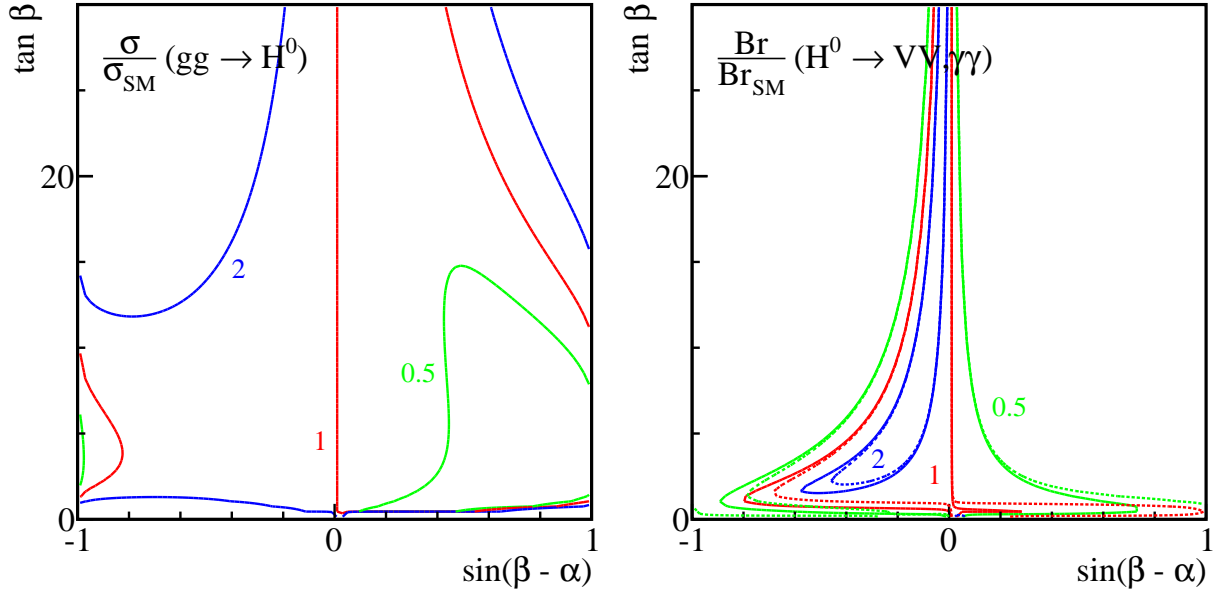


FIG. 11: The normalized $gg \rightarrow H^0$ production cross section contours (left panel) and $H^0 \rightarrow VV$ (solid lines of the right panel) and $H^0 \rightarrow \gamma\gamma$ (dashed lines of the right panel) branching fractions in the H^0 -126 case. The contour lines are $\sigma/\sigma_{\text{SM}}$, $\text{Br}/\text{Br}_{\text{SM}} = 0.5$ (green), 1 (red), and 2 (blue).

Similar to Eqs. (14) and (15) in Sec. IV, the ratios of the gluon fusion cross sections normalized to the SM can be written approximately as:

$$\frac{\sigma(gg \rightarrow H^0)}{\sigma_{\text{SM}}} = \frac{\sin^2 \alpha}{\sin^2 \beta} + \frac{\cos^2 \alpha |A_{1/2}(\tau_b)|^2}{\cos^2 \beta |A_{1/2}(\tau_t)|^2} \quad (17)$$

$$= \left[\frac{\sin(\beta - \alpha)}{\tan \beta} - \cos(\beta - \alpha) \right]^2 + [\sin(\beta - \alpha) \tan \beta + \cos(\beta - \alpha)]^2 \frac{|A_{1/2}(\tau_b)|^2}{|A_{1/2}(\tau_t)|^2}. \quad (18)$$

Contours of $\sigma/\sigma_{\text{SM}}(gg \rightarrow H^0) = 0.5$ (green), 1 (red), and 2 (blue) are shown in the left panel of Fig. 11. H^0 couples exactly like the SM Higgs for $\sin(\beta - \alpha) = 0$, while deviations from the SM values occur for $\sin(\beta - \alpha)$ away from zero. For $\sin(\beta - \alpha) < 0$, $\sigma/\sigma_{\text{SM}}(gg \rightarrow H^0)$ is almost always larger than 1 (except for a small region around $\sin(\beta - \alpha) \sim -1$ and $\tan \beta \lesssim 10$) while a suppression of the gluon fusion production is possible for positive values

of $\sin(\beta - \alpha)$. This is due to cancellations between the $\sin(\beta - \alpha)$ and $\cos(\beta - \alpha)$ terms in the top Yukawa coupling, in particular, for low $\tan \beta$. The bottom loop contributes significantly when $\tan \beta$ is large, which enhances the gluon fusion production cross section.

$\text{Br}(H^0 \rightarrow VV, \gamma\gamma)/\text{Br}_{\text{SM}}$ can also be expressed similar to Eq. (16):

$$\frac{\text{BR}(H^0 \rightarrow XX)}{\text{BR}(h_{\text{SM}} \rightarrow XX)} = \frac{\Gamma_{XX}}{\Gamma_{\text{total}}} \times \frac{\Gamma_{XX}^{\text{SM}}}{\Gamma_{XX}^{\text{SM}}} = \begin{cases} \frac{\cos^2(\beta - \alpha)}{\cos^2(\beta - \alpha)\text{Br}(h_{\text{SM}} \rightarrow VV) + \frac{\cos^2 \alpha}{\cos^2 \beta} \text{Br}(h_{\text{SM}} \rightarrow bb) + \dots} \\ \frac{\Gamma(H^0 \rightarrow \gamma\gamma)/\Gamma(h_{\text{SM}} \rightarrow \gamma\gamma)}{\cos^2(\beta - \alpha)\text{Br}(h_{\text{SM}} \rightarrow VV) + \frac{\cos^2 \alpha}{\cos^2 \beta} \text{Br}(h_{\text{SM}} \rightarrow bb) + \dots} \end{cases}, \quad (19)$$

with the contour lines given in the right panel of Fig. 11. A relative enhancement of the branching fractions over the SM values are observed in extended region of negative $\sin(\beta - \alpha)$, while it is mostly suppressed for positive $\sin(\beta - \alpha)$.

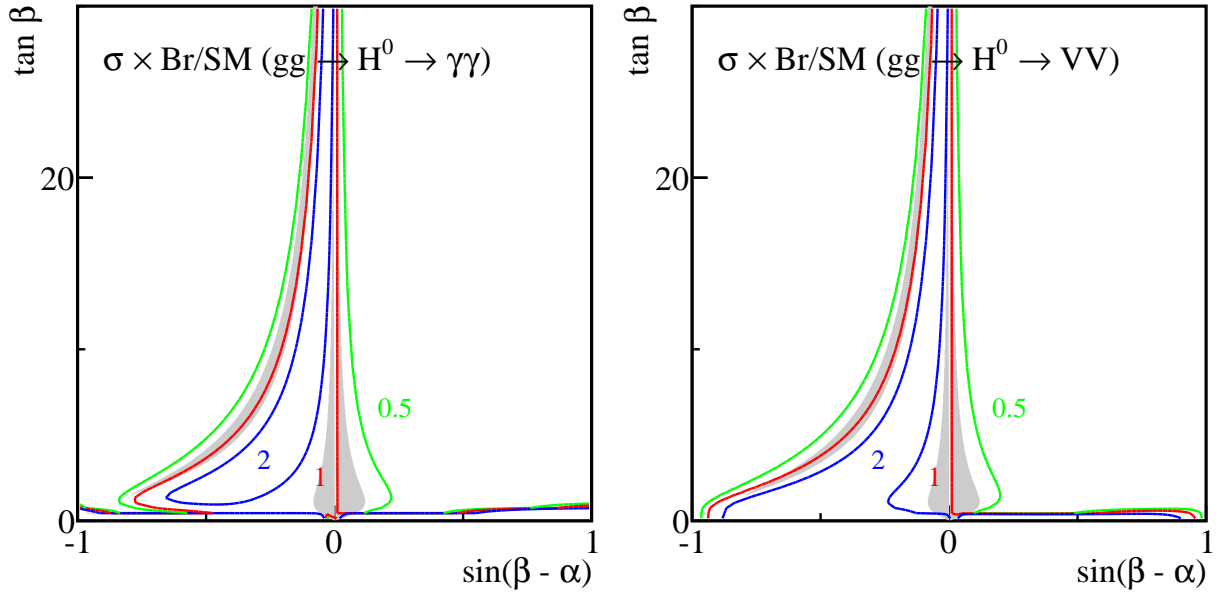


FIG. 12: $\sigma \times \text{Br}/\text{SM}$ for the processes $gg \rightarrow H^0 \rightarrow \gamma\gamma$ (left), and $gg \rightarrow H^0 \rightarrow WW/ZZ$ (right) in the H^0 -126 case. The contour lines are $\sigma \times \text{Br}/\text{SM} = 0.5$ (green), 1 (red), and 2 (blue). The regions where cross sections of $\gamma\gamma$ and WW/ZZ channels satisfy Eq. (12) are shaded gray.

Combining the production cross sections and the decay branching fractions, contours of $gg \rightarrow H^0 \rightarrow XX$ are given in Fig. 12 for $\gamma\gamma$ (left panel) and WW/ZZ channels (right panel). Requiring the cross section to be consistent with the observed Higgs signal: $0.7 - 1.5$ for the $\gamma\gamma$ channel and $0.6 - 1.3$ for the WW/ZZ channel, results in two distinct regions: a region close to $\sin(\beta - \alpha) \sim 0$, and an extended region of $-0.8 \lesssim \sin(\beta - \alpha) \lesssim -0.05$.

Fig. 13 shows the correlation between the $\gamma\gamma$ and VV channels. Most of the points lie

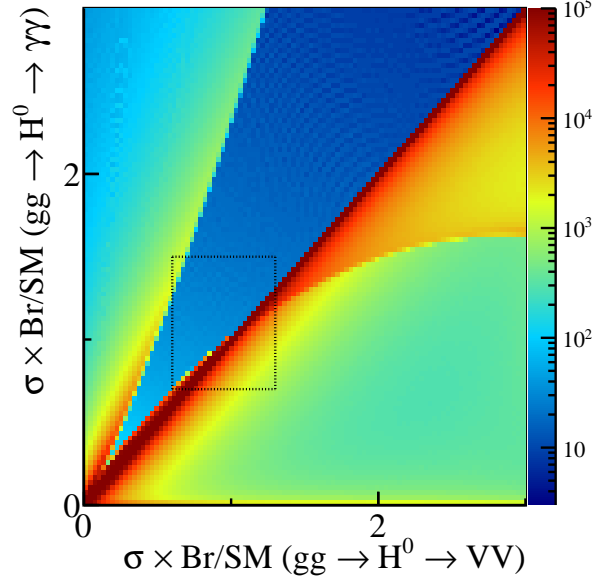


FIG. 13: $\sigma \times \text{Br}/\text{SM}$ for $gg \rightarrow H^0 \rightarrow \gamma\gamma$ versus $gg \rightarrow H^0 \rightarrow VV$ in the H^0 -126 case. Color coding is the same as in Fig. 4. Also indicated by the small rectangular box is the normalized signal cross section range of $\gamma\gamma$ between 0.7 and 1.5, and VV channels between 0.6 and 1.3 [4, 6].

along the diagonal: $\gamma\gamma : VV \sim 1$. A second branch of $\gamma\gamma : WW \sim 2$ also appears, which corresponds to the very low $\tan\beta < 1$ region in Fig. 12. This region is strongly constrained by R_b and flavor bounds, and is therefore not considered further in our study.

B. Parameter Spaces

We now present the results for H^0 -126 case with the full parameter scan, including all the theoretical and experimental constraints. Fig. 14 presents the parameter regions in $\tan\beta$ versus $\sin(\beta - \alpha)$. The color coding is the same as in Fig. 5, except that the signal regions in dark red are those with the heavy CP-even Higgs H^0 interpreted as the observed 126 GeV scalar.

Requiring the heavy CP-even Higgs to satisfy the cross section ranges of the observed Higgs signal results in two signal regions: one region near $\sin(\beta - \alpha) \sim 0$ and an extended region of $-0.8 \lesssim \sin(\beta - \alpha) \lesssim -0.05$, consistent with Fig. 12. Note however that the region around $\sin(\beta - \alpha) \sim 0$ is actually reduced to $\tan\beta \lesssim 8$. This is because larger values of $\tan\beta$ leads to smaller m_h such that $m_h < m_H/2$ (see right panel of Fig. 15 below). The

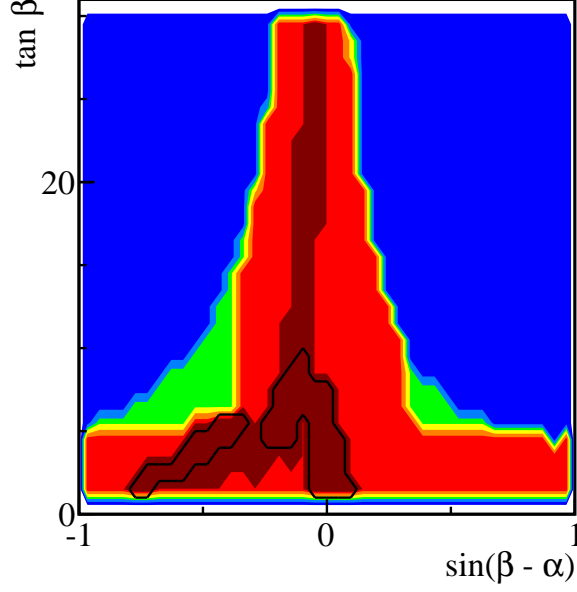


FIG. 14: Parameter regions in the H^0 -126 case for $\tan\beta$ versus $\sin(\beta - \alpha)$. Color coding is the same as Fig. 5 except that the dark red regions are the ones consistent with the heavy CP-even Higgs interpreted as the observed Higgs signal.

opening of $H^0 \rightarrow h^0 h^0$ channel reduces the the branching fractions of $H^0 \rightarrow WW/ZZ, \gamma\gamma$ forcing it outside the signal cross section region. Regions surviving the flavor bounds are the ones enclosed by black curves. Larger values of $\tan\beta \gtrsim 10$ are disfavored.

Fig. 15 shows the parameter region in $\sin(\beta - \alpha)$ versus m_h (left panel) and $\tan\beta$ versus m_h (right panel). Within the narrow region around $\sin(\beta - \alpha) \sim 0$, m_h can take all values up to 126 GeV. For $-0.8 \lesssim \sin(\beta - \alpha) \lesssim -0.35$, when the $H^0 WW, H^0 ZZ$ couplings could significantly deviate from the SM value while $h^0 WW, h^0 ZZ$ couplings are sizable, the light CP-even Higgs mass is constrained to be larger than about 80 GeV from LEP Higgs searches [37, 38]. This is the interesting region where the two Higgses are close to being degenerate, with both h^0 and H^0 showing significant deviation of their couplings to gauge bosons from the SM value.

The right panel of Fig. 15 shows the parameter region of $\tan\beta$ versus m_h . Larger values of $\tan\beta$ is only allowed for small values of m_h . The red region where $m_h < 60$ GeV and $\tan\beta \lesssim 5$ can not satisfy the Higgs signal cross section requirement due to the opening of $H^0 \rightarrow h^0 h^0$ mode, which corresponds to the $m_h < 60$ GeV, $\sin(\beta - \alpha) \sim 0$ red region in the $\sin(\beta - \alpha)$ versus m_h plot (left panel of Fig. 15). Imposing the flavor bounds further rules

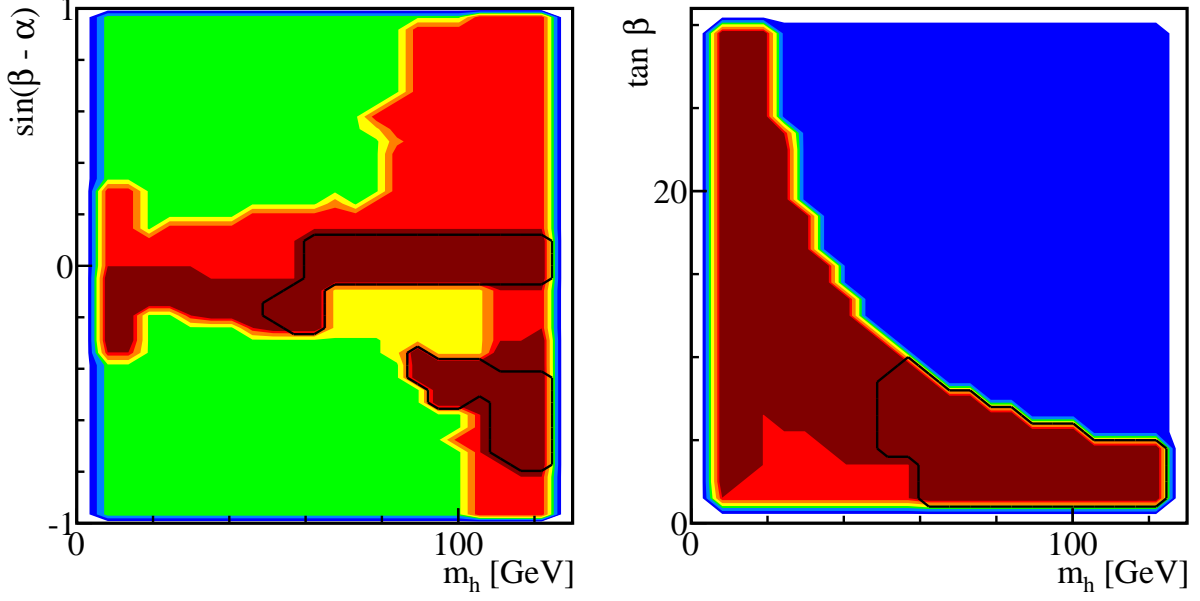


FIG. 15: Parameter regions in the H^0 -126 case for $\sin(\beta - \alpha)$ versus m_h (left panel) and $\tan \beta$ versus m_h (right panel). Color coding is the same as Fig. 14.

out regions with light m_h below about 50 GeV, mainly due to the process $B_s \rightarrow \mu^+ \mu^-$, as shown in the right panel of Fig. 1. Large values of $\tan \beta \gtrsim 10$ are excluded correspondingly.

Fig. 16 shows $\sin(\beta - \alpha)$ versus m_{A,H^\pm} (left panels) and $\tan \beta$ versus m_{A,H^\pm} (right panels). The plots for m_A and m_{H^\pm} are very similar, except for very low masses. Very large values of $m_{A,H^\pm} \gtrsim 800$ GeV are excluded by theoretical considerations, similar to the h^0 -126 case. $m_A \lesssim 60$ GeV and $\tan \beta \gtrsim 5$ are excluded by the LEP Higgs search [37], while the triangle region of $130 \lesssim m_A \lesssim 400$ GeV and $\tan \beta \gtrsim 13$ is excluded by the LHC searches for the CP-odd Higgs in $\tau\tau$ mode [42, 43]. For the charged Higgs, small values of $m_{H^\pm} \lesssim 80$ GeV are ruled out by LEP searches on charged Higgs [39, 40]. Tevatron and the LHC charged Higgs searches [42, 43]: $t \rightarrow H^\pm b \rightarrow \tau \nu_\tau b$ further rule out regions of $m_{H^\pm} \lesssim 150$ GeV and $\tan \beta \gtrsim 17$. The triangle in m_{H^\pm} versus $\tan \beta$ plot for $150 \text{ GeV} \lesssim m_{H^\pm} \lesssim 400$ GeV and $\tan \beta \gtrsim 13$ is translated from the corresponding region in $\tan \beta$ versus m_A , due to the correlation between m_A and m_{H^\pm} introduced by $\Delta\rho$, as shown below in Fig. 17. Imposing the flavor constraints further limits $m_A \gtrsim 300$ GeV, $m_{H^\pm} \gtrsim 300$ GeV and $\tan \beta \lesssim 10$.

m_A and m_{H^\pm} exhibit a much stronger correlation in the H^0 -126 case, mostly due to the $\Delta\rho$ constraints, as shown in the left panel of Fig. 17. Comparing with the h^0 -126 case, in which m_H could be large with a relaxed constraints on m_A and m_{H^\pm} mass correlation, in the

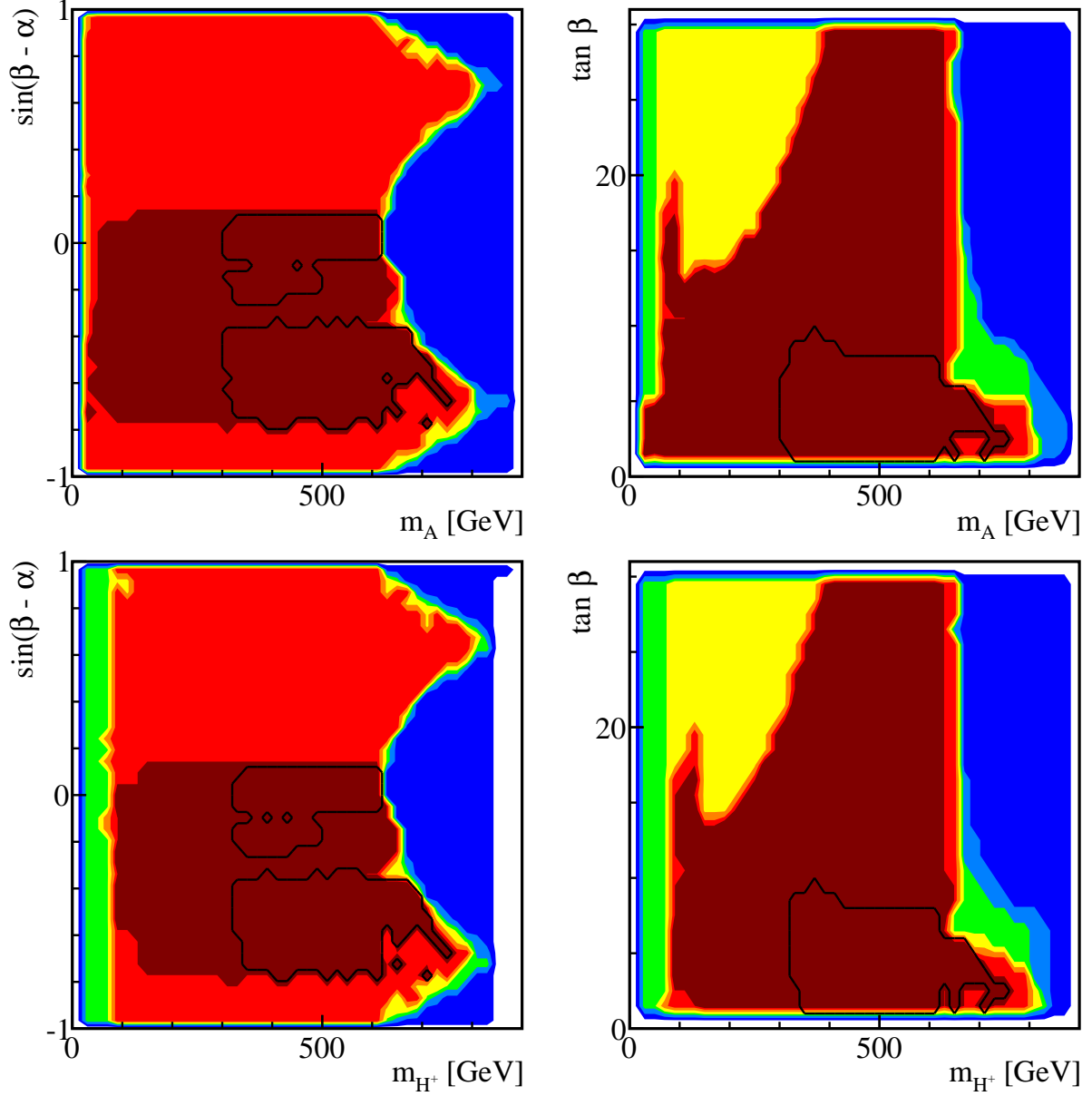


FIG. 16: Parameter regions in the H^0 -126 case for $\sin(\beta - \alpha)$ versus m_A (upper left panel) and $\tan \beta$ versus m_A (upper right panel), as well as similar plots for m_{H^\pm} (lower panels). Color coding is the same as Fig. 14.

H^0 -126 case, both m_h and m_H are relatively small. m_A and m_{H^\pm} should therefore be highly correlated in order to avoid large custodial symmetry breaking in the Higgs sector. However, there is a small strip of allowed region at $m_{H^\pm} \sim 100$ GeV with m_A between 200 – 700 GeV. This region escapes the $\Delta\rho$ constraint since for $m_{H^\pm} \sim m_h \sim m_H$, the contribution to $\Delta\rho$ introduced by the large mass difference between m_A and m_{H^\pm} is cancelled by the (h^0, A^0)

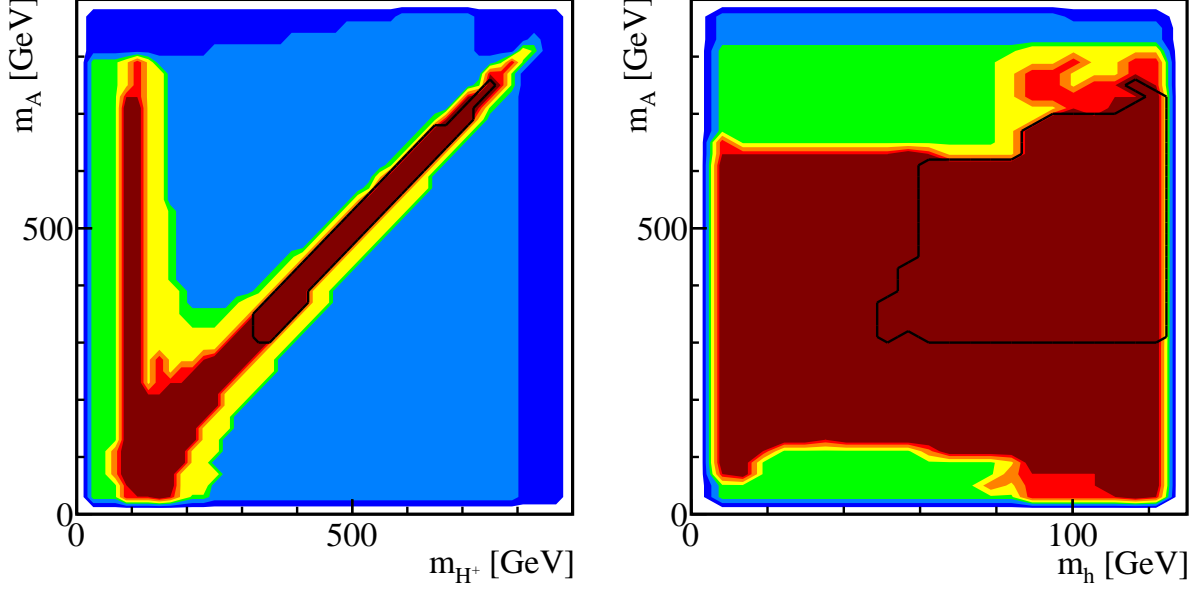


FIG. 17: Parameter regions in the H^0 -126 case for m_A versus m_{H^\pm} (left panel) and m_h (right panel). Color coding is the same as Fig. 14.

loop and (H^0, A^0) loop. Imposing the flavor constraints again limits m_{H^\pm} to be larger than 300 GeV. m_A is constrained to be more than 300 GeV as well due to the correlations.

The right panel of Fig. 17 shows the parameter region of m_A versus m_h , which does not show much correlation. For $m_h \lesssim 90$ GeV, low values of $m_A \lesssim 100$ GeV is excluded by LEP searches of $h^0 A^0$ channel [37]. High values of $m_A \gtrsim 600$ GeV are excluded for $m_h < 90$ GeV. This is because such a large value of m_A can only be realized for $|\sin(\beta - \alpha)| > 0.3$ (see the upper-left panel of Fig. 16). Such regions of $|\sin(\beta - \alpha)| > 0.3$ and $m_h < 90$ GeV are excluded by the LEP Higgs search of $h^0 Z$ channel [38], as shown clearly in the m_h versus $\sin(\beta - \alpha)$ plot (left panel of Fig. 15). Such excluded regions for large m_A (and large m_{H^\pm} due to correlation) also appears in the $\tan \beta$ versus m_A (m_{H^\pm}) plots in Fig. 16.

We end the section with the following observations:

- Contrary to the h^0 -126 case, fixing the heavy CP-even Higgses to be the 126 GeV resonance forces us into a small narrow region of $\sin(\alpha - \beta) \sim 0$ with $\tan \beta \lesssim 8$ or an extended region of $-0.8 \lesssim \sin(\alpha - \beta) \lesssim -0.05$ with less restrictions on $\tan \beta$.
- The light CP-even Higgs can have mass of any value up to 126 GeV, with smaller m_h only allowed for $\sin(\beta - \alpha) \sim 0$. Note that the case of nearly degenerate h^0 and H^0 is allowed, as studied in detail in Ref. [21].

- m_A and m_{H^\pm} exhibit a strong correlation: $m_A \simeq m_{H^\pm}$, due to $\Delta\rho$ constraints.
- Flavor bounds impose the strong constraints: $\tan\beta \lesssim 10$, $m_h > 50$ GeV, and $m_{H^\pm} > 300$ GeV. m_A is also constrained to be more than 300 GeV due to the correlation between m_A and m_{H^\pm} .

VI. OTHER HIGGS CHANNELS

Thus far, we have concentrated on the gluon fusion production mechanism and the dominant $\gamma\gamma$, ZZ and WW decay channels for the Higgs. The vector boson fusion channel is another important production channel for the CP-even Higgses. For certain Higgs decay channels, for example, $\tau\tau$ mode, VBF production is the one that provides the dominant sensitivity due to the excellent discrimination of the backgrounds using the two forward tagging jets and the central jet-veto [60]. Other production channels, VH and ttH associated production, can also be of interest for Higgs decay to bb . In this section, we discuss the cross sections in other search channels for both h^0 and H^0 when they are interpreted as the observed 126 GeV scalar.

In Fig. 18, we show the normalized cross sections for the WW/ZZ , $\gamma\gamma$ (left panel) and $bb/\tau\tau$ (right panel) final states via VBF or VH associated production (both production cross sections are controlled by h^0VV coupling) in the $\tan\beta$ versus $\sin(\beta - \alpha)$ plane for the h^0 -126 case. For $VBF/VH \rightarrow h^0 \rightarrow WW/ZZ$, both the production and decay are proportional to $\sin(\beta - \alpha)$, resulting in regions highly centered around $\sin(\beta - \alpha) \sim \pm 1$ for any enhancement above the SM value. For the currently preferred gray Higgs signal regions, $VBF/VH \rightarrow h^0 \rightarrow WW/ZZ$ is typically in the range of 0.5 – 1 of the SM value.

The current observation of the Higgs signal has been fitted into the signal strength in both the gluon fusion channel and VBF channel for $\gamma\gamma$, WW and ZZ final states [4–6]. Imposing the 95% C.L. contours of the $\mu_{ggF+ttH} \times B/B_{\text{SM}}$ versus $\mu_{VBF+VH} \times B/B_{\text{SM}}$ on top of the one-dimensional gluon fusion signal regions as given in Eq. (12) does not lead to additional reduction of the signal parameter space, given the VBF channel is relatively loosely constrained.

For $VBF/VH \rightarrow h^0 \rightarrow bb/\tau\tau$, the cross section is suppressed for most of the regions, except in the neighborhood of $\sin(\beta - \alpha) = \pm 1$ where SM rates can be achieved. The current preferred signal regions typically have a suppression of 0.5 or stronger for this $bb/\tau\tau$ channel.

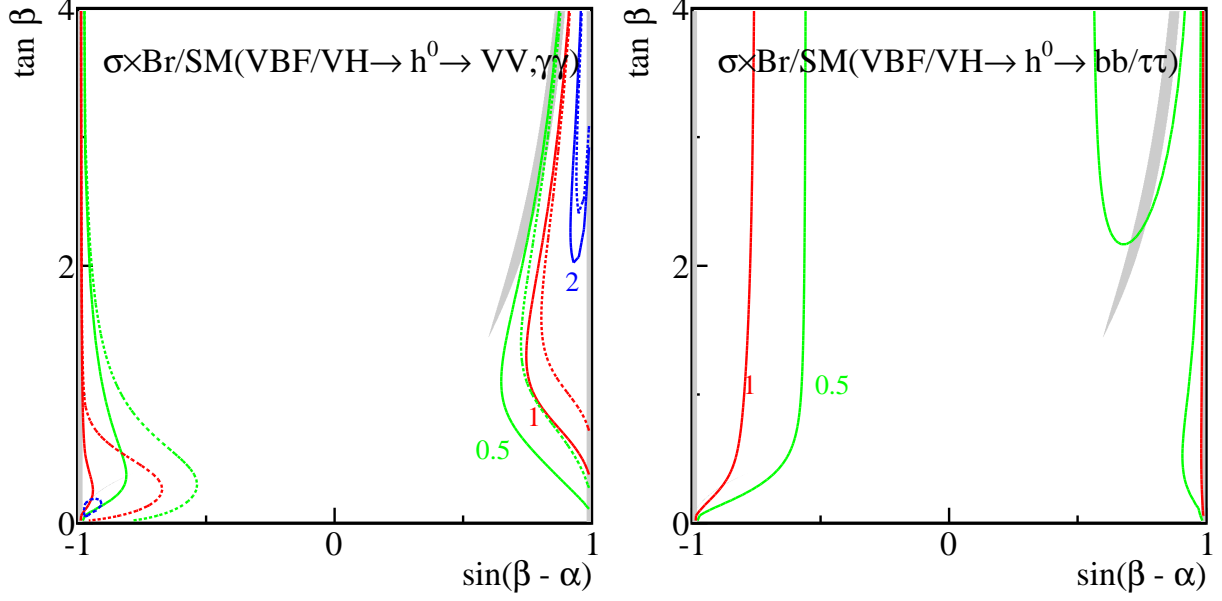


FIG. 18: $\sigma \times \text{Br}/\text{SM}$ for $\text{VBF}/\text{VH} \rightarrow h^0 \rightarrow \text{WW}/\text{ZZ}$ (solid curves in left panel), $\gamma\gamma$ (dashed curves in left panel) and $\text{VBF}/\text{VH} \rightarrow h^0 \rightarrow \text{bb}/\tau\tau$ (right panel) for the h^0 -126 case. The contour lines show $\sigma \times \text{Br}/\text{SM} = 0.5$ (green), 1 (red) and 2 (blue). The shaded gray regions correspond to the signal regions where cross sections of $\gamma\gamma$ and WW/ZZ channels satisfy Eq. (12) as well as R_b .

There is also a strong inverse correlation between the WW/ZZ and $\text{bb}/\tau\tau$ channels, since an increase in bb decay branching fraction can only occur at the expense of WW . Given the relatively loose bounds on the signal strength in the bb and $\tau\tau$ channels from the LHC and the Tevatron experiments [4, 61–64], imposing the current search results for bb and $\tau\tau$ channels does not lead to further reduction of the signal parameter space.

Fig. 19 show the $\sigma \times \text{Br}/\text{SM}$ plots for VV , $\gamma\gamma$, and $\text{bb}/\tau\tau$ channel via VBF/VH production for the H^0 -126 case. The qualitative features of the VV , $\gamma\gamma$ plot is the same as that of Fig. 12. The currently favored gray signal regions typically correspond to a normalized cross section of $\text{VBF}/\text{VH} \rightarrow H^0 \rightarrow \text{WW}/\text{ZZ}$ around 1 as well.

The $\text{bb}/\tau\tau$ channel, however, exhibits a very different behavior. For two regions of $-0.6 \leq \sin(\beta - \alpha) \leq -0.1$ and $0 \leq \sin(\beta - \alpha) \leq 0.6$ (regions enclosed by the red curves in the right panel of Fig. 19), a normalized cross section of at least the SM signal strength can be achieved. A strong suppression, sometime as small as 0.1, can be obtained in the other regions. The currently favored gray signal region near $\sin(\beta - \alpha) \sim 0$ corresponds to $\sigma/\sigma_{\text{SM}}$ of order 1 for $\text{VBF}/\text{VH} \rightarrow H^0 \rightarrow \text{bb}/\tau\tau$ channel, while a suppression as large as 0.5 is

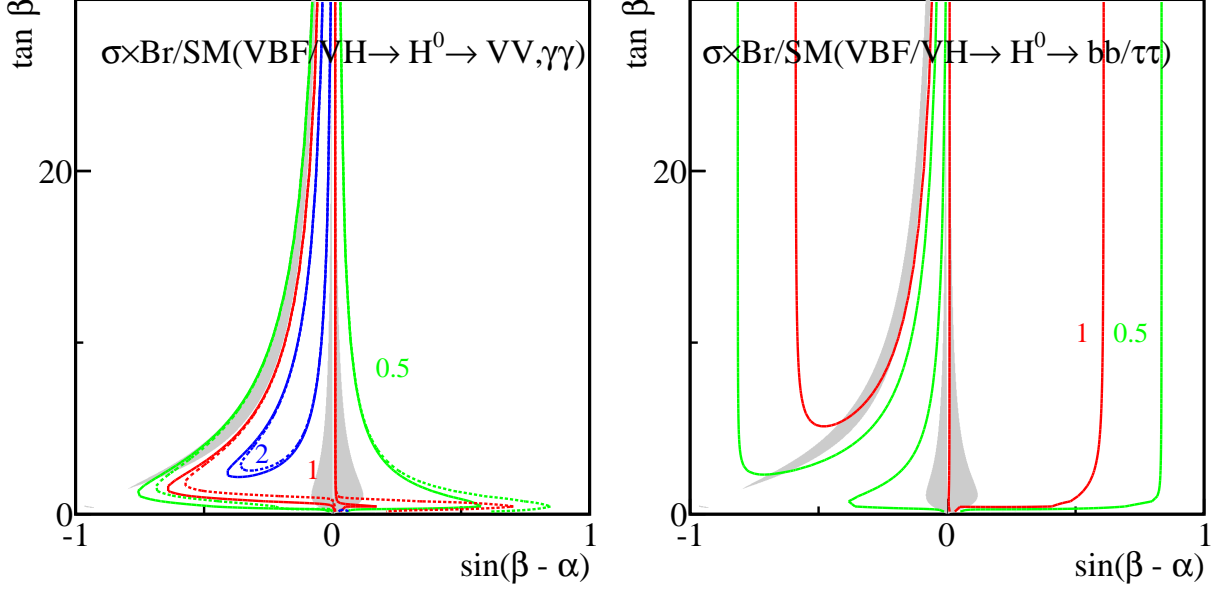


FIG. 19: $\sigma \times \text{Br}/\text{SM}$ for $VBF/VH \rightarrow H^0 \rightarrow WW/ZZ, \gamma\gamma$ (left) and $VBF/VH \rightarrow H^0 \rightarrow bb/\tau\tau$ (right) for the H^0 -126 case. Color coding is the same as in Fig. 18.

possible for the extended regions in negative $\sin(\beta - \alpha)$. The inverse correlation between $bb/\tau\tau$ and WW channels also appears in the H^0 -126 case. Similar to the h^0 -126 case, imposing the 95% C.L. range for the VBF process for $\gamma\gamma$ and WW/ZZ channel, as well as the signal strength obtained from the bb and $\tau\tau$ modes does not lead to further reduction of the signal region.

We also studied $gg \rightarrow h^0, H^0 \rightarrow bb/\tau\tau$ channel for both the h^0 -126 and H^0 -126 cases, and noticed that for the currently favored Higgs signal regions, a factor of 2 enhancement could be realized.

VII. CONCLUSIONS

In this paper, we presented a detailed analysis of the Type II 2HDM (with an imposed Z_2 symmetry) parameter space, identifying either the light or the heavy CP-even Higgs as the recently discovered resonance at 126 GeV. We scanned the remaining five parameters $\sin(\beta - \alpha)$, $\tan \beta$, m_A , m_{H^\pm} , and m_H or m_h while fixing either m_h or m_H to be 126 GeV. We took into account all the theoretical constraints, precision measurements, as well as current experimental search limits on the Higgses. We further studied the implications on

the parameter space once flavor constraints are imposed. We found unique features in each of these two cases.

In the h^0 -126 case, we are forced into regions of parameter space where $\sin(\beta - \alpha) = \pm 1$ with $\tan \beta$ between 0.5 to 4, or an extended region of $0.55 < \sin(\beta - \alpha) < 0.9$, with $\tan \beta$ constrained to be in the range of 1.5 to 4. There is, however, a wide range of values that are still allowed for the masses of the heavy CP-even, pseudo scalar and charged Higgses. The Higgs masses are typically not correlated, except when $m_{A,H^\pm} \gtrsim 600$ GeV and $\sin(\beta - \alpha) > 0$ where there is a strong correlation between m_A and m_{H^\pm} because of the $\Delta\rho$ constraint. Imposing flavor constraints further restricts $m_{H^\pm} > 300$ GeV.

In the H^0 -126 case, we are forced into an orthogonal region of parameter space where $\sin(\beta - \alpha) \sim 0$, $\tan \beta \lesssim 8$ or an extended region of $-0.8 \lesssim \sin(\alpha - \beta) \lesssim -0.05$ with less restricted $\tan \beta$. m_A and m_{H^\pm} exhibit strong correlations: $m_A \simeq m_{H^\pm}$, due to the $\Delta\rho$ constraint. The interesting scenario of the light CP-even Higgs being close to 126 GeV still survives. Imposing flavor bounds further shrinks the parameter space considerably: $\tan \beta \lesssim 10$, $m_h > 50$ GeV, $m_{H^\pm} > 300$ GeV, and $m_A > 300$ GeV.

Note that in both cases, the extended region in $\sin(\beta - \alpha)$ is of particular interest, since a deviation of the Higgs coupling to WW and ZZ can be accommodated for the observed Higgs signal at 126 GeV.

We find that in either of these scenarios, one can identify regions of parameter space that pass all theoretical and experimental bounds and still allow a slightly higher than SM rate to diphotons. $\gamma\gamma$ and WW/ZZ rates are most likely strongly correlated: $\gamma\gamma : VV \sim 1$ for the normalized cross sections.

We further studied the implication for the Higgs production via VBF or VH process, and decays to bb , $\tau\tau$ channels. We found that in the h^0 -126 case, both $VBF/VH \rightarrow h^0 \rightarrow bb/\tau\tau, WW/ZZ$ could be significantly suppressed in the Higgs signal region. For the H^0 -126 case, $VBF/VH \rightarrow H^0 \rightarrow WW/ZZ$ channel is almost the SM strength. Possible suppression of $bb/\tau\tau$ channel up to 0.5 is possible for the extended signal regions in negative $\sin(\beta - \alpha)$. Future observation of the bb and $\tau\tau$ modes can provide valuable information for the parameter regions of the type II 2HDM.

Comparing to the MSSM, with its Higgs sector being a restricted type II 2HDM and the tree level Higgs spectrum completely determined by m_A and $\tan \beta$, the parameter regions of the general Type II 2HDM is much more relaxed. Unlike the MSSM in which the h^0 -126

case corresponds to the decoupling region where $m_A \gtrsim 300$ GeV, and the H^0 -126 GeV case corresponds to the non-decoupling region where $m_A \sim 100 - 130$ GeV [65], the value of m_A in the general Type II 2HDM could vary over the entire viable region up to about 800 GeV. The MSSM relation of $m_A \sim m_{H^\pm} \sim m_H$ in the decoupling region is also much more relaxed in the Type II 2HDM. No obvious correlation is observed between m_A , m_{H^\pm} , and m_H for the h^0 -126 case, except for the region with large $m_{A,H^\pm} \gtrsim 600$ GeV. Note also that in the Type II 2HDM with Z_2 symmetry (such that $m_{12} = 0$) that we are considering, with the additional perturbativity and unitarity constraints imposed, there is an upper limit of about 800 GeV for the mass of H^0 , A^0 and H^\pm . The presence of an upper bound on the heavy Higgs masses reiterates our point that unlike the MSSM, there is no sensible decoupling limit in this case where only one light SM-like Higgs appears in the low energy spectrum with other Higgses heavy and decouple.

Observations of extra Higgses in the future would further pin down the Higgs sector beyond the SM. While the conventional decay channels of Higgses to SM particles continue to be important channels to search for extra Higgses, novel decay channels of a heavy Higgs into light Higgses or light Higgs plus gauge boson could also appear. Future work along the lines of collider phenomenology of multiple Higgs scenarios is definitely warranted.

Acknowledgments

We thank L. Carpenter for her participation at the beginning of this project. We would also like to thank David Lopez-Val for useful discussions and Oscar Stål for sharing the 2HDMC package. This work was supported by the Department of Energy under Grant DE-FG02-04ER-41298.

-
- [1] G. Aad *et al.* [ATLAS Collaboration], Phys. Lett. B **716**, 1 (2012) [arXiv:1207.7214 [hep-ex]].
 - [2] ATLAS Collaboration, G. Aad *et al.*, *Combined measurements of the mass and signal strength of the Higgs-like boson with the ATLAS detector using up to 25 fb⁻¹ of proton-proton collision data*, Tech. Rep. ATLAS-CONF-2013-014.
 - [3] S. Chatrchyan *et al.* [CMS Collaboration], Phys. Lett. B **716**, 30 (2012) [arXiv:1207.7235 [hep-ex]].

- [4] CMS Collaboration, S. Chatrchyan et al., *Combination of standard model Higgs boson searches and measurements of the properties of the new boson with a mass near 125 GeV*, Tech. Rep. CMS-PAS-HIG-13-005.
- [5] ATLAS Collaboration, G. Aad et al., *Study of the spin of the new boson with up to 25 fb⁻¹ of ATLAS data*, Tech. Rep. ATLAS-CONF-2013-040; *Combined coupling measurements of the Higgs-like boson with the ATLAS detector using up to 25 fb⁻¹ of proton-proton collision data*, Tech. Rep. ATLAS-CONF-2013-034.
- [6] G. Aad *et al.* [ATLAS Collaboration], Phys. Lett. B (2013) [arXiv:1307.1427 [hep-ex]].
- [7] G. C. Branco, P. M. Ferreira, L. Lavoura, M. N. Rebelo, M. Sher and J. P. Silva, Phys. Rept. **516**, 1 (2012) [arXiv:1106.0034 [hep-ph]].
- [8] H.E. Haber, G.L. Kane and T. Sterling, Nucl. Phys. **B161**, 493 (1979).
- [9] L.J. Hall and M.B. Wise, Nucl. Phys. **B187**, 397 (1981).
- [10] J.F. Donoghue and L.F. Li, Phys. Rev. **D19**, 945 (1979).
- [11] P. M. Ferreira, R. Santos, M. Sher and J. P. Silva, Phys. Rev. D **85**, 077703 (2012) [arXiv:1112.3277 [hep-ph]].
- [12] P. M. Ferreira, R. Santos, M. Sher and J. P. Silva, Phys. Rev. D **85**, 035020 (2012) [arXiv:1201.0019 [hep-ph]].
- [13] H. S. Cheon and S. K. Kang, arXiv:1207.1083 [hep-ph].
- [14] A. Drozd, B. Grzadkowski, J. F. Gunion and Y. Jiang, arXiv:1211.3580 [hep-ph].
- [15] S. Chang, S. K. Kang, J. -P. Lee, K. Y. Lee, S. C. Park and J. Song, arXiv:1210.3439 [hep-ph].
- [16] C. -Y. Chen and S. Dawson, arXiv:1301.0309 [hep-ph].
- [17] B. Grinstein and P. Uttayarat, arXiv:1304.0028 [hep-ph].
- [18] C. -W. Chiang and K. Yagyu, arXiv:1303.0168 [hep-ph].
- [19] N. Craig and S. Thomas, JHEP **1211**, 083 (2012) [arXiv:1207.4835 [hep-ph]].
- [20] L. Basso, A. Lipniacka, F. Mahmoudi, S. Moretti, P. Osland, G. M. Pruna and M. Purmohammadi, JHEP **1211**, 011 (2012) [arXiv:1205.6569 [hep-ph]].
- [21] P. M. Ferreira, H. E. Haber, R. Santos and J. P. Silva, arXiv:1211.3131 [hep-ph].
- [22] G. Burdman, C. E. F. Haluch and R. D. Matheus, Phys. Rev. D **85**, 095016 (2012) [arXiv:1112.3961 [hep-ph]].
- [23] E. Cervero and J. -M. Gerard, Phys. Lett. B **712**, 255 (2012) [arXiv:1202.1973 [hep-ph]].
- [24] J. Shu and Y. Zhang, arXiv:1304.0773 [hep-ph].

- [25] B. Coleppa, K. Kumar and H. E. Logan, Phys. Rev. D **86**, 075022 (2012) [arXiv:1208.2692 [hep-ph]].
- [26] S. Davidson and H. E. Haber, Phys. Rev. D **72**, 035004 (2005) [Erratum-ibid. D **72**, 099902 (2005)] [hep-ph/0504050]; H. E. Haber and D. O’Neil, Phys. Rev. D **74**, 015018 (2006) [hep-ph/0602242].
- [27] I. F. Ginzburg and M. Krawczyk, Phys. Rev. D **72**, 115013 (2005) [hep-ph/0408011].
- [28] D. Eriksson, J. Rathsmann and O. Stal, Comput. Phys. Commun. **181**, 189 (2010) [arXiv:0902.0851 [hep-ph]].
- [29] P. Bechtle, O. Brein, S. Heinemeyer, G. Weiglein and K. Williams, AIP Conf. Proc. **1200**, 510 (2010) [arXiv:0909.4664 [hep-ph]];
- [30] P. Bechtle, O. Brein, S. Heinemeyer, G. Weiglein and K. E. Williams, PoS CHARGED **2010**, 027 (2010) [arXiv:1012.5170 [hep-ph]];
- [31] P. Bechtle, O. Brein, S. Heinemeyer, G. Weiglein and K. E. Williams, Comput. Phys. Commun. **181**, 138 (2010) [arXiv:0811.4169 [hep-ph]]; P. Bechtle, O. Brein, S. Heinemeyer, G. Weiglein and K. E. Williams, Comput. Phys. Commun. **182**, 2605 (2011) [arXiv:1102.1898 [hep-ph]]; P. Bechtle, O. Brein, S. Heinemeyer, O. Stal, T. Stefaniak, G. Weiglein and K. Williams, PoS CHARGED **2012**, 024 (2012) [arXiv:1301.2345 [hep-ph]].
- [32] N. G. Deshpande and E. Ma, Phys. Rev. D **18**, 2574 (1978); M. Sher, Phys. Rept. **179**, 273 (1989); A. W. El Kaffas, W. Khater, O. M. Ogreid and P. Osland, Nucl. Phys. B **775**, 45 (2007) [hep-ph/0605142].
- [33] J. Bijnens, J. Lu and J. Rathsmann, JHEP **1205**, 118 (2012) [arXiv:1111.5760 [hep-ph]].
- [34] I. F. Ginzburg and I. P. Ivanov, Phys. Rev. D **72**, 115010 (2005) [hep-ph/0508020].
- [35] ATLAS Collaboration, G. Aad et al., *Measurements of the properties of the Higgs-like boson in the $WW(*) \rightarrow l\nu l\nu$ decay channel with the ATLAS detector using 25 fb⁻¹ of proton-proton collision data*, Tech. Rep. ATLAS-CONF-2013-030; *Measurements of the properties of the Higgs-like boson in the two photon decay channel with the ATLAS detector using 25 fb⁻¹ of proton-proton collision data*, Tech. Rep. ATLAS-CONF-2013-012; *Measurements of the properties of the Higgs-like boson in the four lepton decay channel with the ATLAS detector using 25 fb⁻¹ of proton-proton collision data*, Tech. Rep. ATLAS-CONF-2013-013; *Search for the Standard Model Higgs boson produced in association with top quarks in proton-proton collisions at $\sqrt{s} = 7\text{TeV}$ using the ATLAS detector*, Tech. Rep. ATLAS-CONF-2012-135; Phys.

- Lett. B **718**, 369 (2012) [arXiv:1207.0210 [hep-ex]]; JHEP **1209**, 070 (2012) [arXiv:1206.5971 [hep-ex]].
- [36] CMS Collaboration, S. Chatrchyan et al., *Updated measurements of the Higgs boson at 125 GeV in the two photon decay channel*, Tech. Rep. CMS-PAS-HIG-13-001; *Properties of the Higgs-like boson in the decay H to ZZ to $4l$ in pp collisions at $\sqrt{s}=7$ and 8 TeV*, Tech. Rep. CMS-PAS-HIG-13-002; *Evidence for a particle decaying to $W+W^-$ in the fully leptonic final state in a standard model Higgs boson search in pp collisions at the LHC*, Tech. Rep. CMS-PAS-HIG-13-003; *Search for the Standard-Model Higgs boson decaying to tau pairs in proton-proton collisions at $\sqrt{s}=7$ and 8 TeV*, Tech. Rep. CMS-PAS-HIG-13-004; *Search for Higgs boson production in association with top quark pairs in pp collisions*, Tech. Rep. CMS-PAS-HIG-12-025; *Search for the standard model Higgs boson produced in association with W or Z bosons, and decaying to bottom quarks for HCP 2012*, Tech. Rep. CMS-PAS-HIG-12-044.
- [37] ALEPH Collaboration, DELPHI Collaboration, L3 Collaboration, OPAL Collaboration, LEP Working Group for Higgs Boson Searches Collaboration, S. Schael et al., *Search for neutral MSSM Higgs bosons at LEP*, *Eur.Phys.J.* **C47** (2006) 547–587, [hep-ex/0602042].
- [38] LEP Working Group for Higgs boson searches, ALEPH Collaboration, DELPHI Collaboration, L3 Collaboration, OPAL Collaboration, R. Barate et al., *Search for the standard model Higgs boson at LEP*, *Phys.Lett.* **B565** (2003) 61–75, [hep-ex/0306033].
- [39] LEP Higgs Working Group for Higgs boson searches, ALEPH Collaboration, DELPHI Collaboration, L3 Collaboration, OPAL Collaboration, *Search for charged Higgs bosons: Preliminary combined results using LEP data collected at energies up to 209-GeV*, [hep-ex/0107031].
- [40] ALEPH Collaboration, A. Heister et al., *Search for charged Higgs bosons in e^+e^- collisions at energies up to $\sqrt{s}=209$ -GeV*, *Phys.Lett.* **B543** (2002) 1–13, [[hep-ex/0207054]].
- [41] Tevatron New Physics Higgs Working Group and CDF and D0 Collaborations, arXiv:1207.0449 [hep-ex].
- [42] ATLAS Collaboration, G. Aad et al., *Search for Neutral MSSM Higgs bosons in $\sqrt{s}=7$ TeV pp collisions at ATLAS*, Tech. Rep. ATLAS-CONF-2012-094. JHEP **1206**, 039 (2012) [arXiv:1204.2760 [hep-ex]]; arXiv:1302.3694 [hep-ex].
- [43] S. Chatrchyan et al. [CMS Collaboration], *Phys. Lett. B* **713**, 68 (2012) [arXiv:1202.4083 [hep-ex]]; *Higgs to tau tau (MSSM) (HCP)*, Tech. Rep. CMS-PAS-HIG-12-050; arXiv:1302.2892

- [hep-ex]; JHEP **1207**, 143 (2012) [arXiv:1205.5736 [hep-ex]].
- [44] M. E. Peskin and T. Takeuchi, Phys. Rev. Lett. **65**, 964 (1990).
- [45] J. F. Gunion, H. E. Haber, G. Kane, S. Dawson, *The Higgs Hunter's Guide*, Addison-Wesley Publishing Company, 1990.
- [46] K. Nakamura *et al.* [Particle Data Group Collaboration], J. Phys. G **37**, 075021 (2010).
- [47] H. E. Logan, hep-ph/9906332.
- [48] [ALEPH and CDF and D0 and DELPHI and L3 and OPAL and SLD and LEP Electroweak Working Group and Tevatron Electroweak Working Group and SLD Electroweak and Heavy Flavour Groups Collaborations], arXiv:1012.2367 [hep-ex].
- [49] F. Mahmoudi, Comput. Phys. Commun. **180**, 1579 (2009) [arXiv:0808.3144 [hep-ph]].
- [50] J. Beringer *et al.* (Particle Data Group), Phys. Rev. D **86**, 010001 (2012), and 2013 partial update for the 2014 edition.
- [51] Y. Amhis *et al.* [Heavy Flavor Averaging Group Collaboration], arXiv:1207.1158 [hep-ex], and online updates at <http://www.slac.stanford.edu/xorg/hfag>.
- [52] I. Adachi *et al.* [Belle Collaboration], Phys. Rev. Lett. **110**, 131801 (2013) [arXiv:1208.4678 [hep-ex]].
- [53] P. del Amo Sanchez *et al.* [BaBar Collaboration], Phys. Rev. D **82**, 091103 (2010) [arXiv:1008.4080 [hep-ex]].
- [54] R. Aaij *et al.* [LHCb Collaboration], Phys. Rev. Lett. **111**, 101805 (2013) [arXiv:1307.5024 [hep-ex]].
- [55] B. Aubert *et al.* [BaBar Collaboration], Phys. Rev. Lett. **96**, 241802 (2006) [hep-ex/0511015].
- [56] F. Mahmoudi and O. Stal, Phys. Rev. D **81**, 035016 (2010) [arXiv:0907.1791 [hep-ph]].
- [57] J. P. Lees *et al.* [BaBar Collaboration], Phys. Rev. Lett. **109**, 101802 (2012) [arXiv:1205.5442 [hep-ex]].
- [58] M. Tanaka and R. Watanabe, Phys. Rev. D **82**, 034027 (2010) [arXiv:1005.4306 [hep-ph]].
- [59] V. D. Barger, J. L. Hewett and R. J. N. Phillips, Phys. Rev. D **41**, 3421 (1990).
- [60] D. L. Rainwater, D. Zeppenfeld and K. Hagiwara, Phys. Rev. D **59**, 014037 (1998) [hep-ph/9808468].
- [61] CMS Collaboration, S. Chatrchyan *et al.*, *Search for Higgs Boson production in association with a top-quark pair and decaying to bottom quarks or tau leptons*, Tech. Rep. CMS-PAS-HIG-13-019.

- [62] ATLAS Collaboration, G. Aad et al., *Search for the bb decay of the Standard Model Higgs boson in associated W/ZH production with the ATLAS detector*, Tech. Rep. ATLAS-CONF-2013-079.
- [63] ATLAS Collaboration, G. Aad et al., *Search for the Standard Model Higgs boson produced in association with top quarks in proton-proton collisions at $s = 7$ TeV using the ATLAS detector*, Tech. Rep. ATLAS-CONF-2012-135.
- [64] T. Aaltonen *et al.* [CDF and D0 Collaborations], arXiv:1303.6346 [hep-ex].
- [65] N. D. Christensen, T. Han and S. Su, Phys. Rev. D **85**, 115018 (2012) [arXiv:1203.3207 [hep-ph]].